

Precise predictions for $t\bar{t}\gamma/t\bar{t}$ cross section ratios at the LHC

G. Bevilacqua,^a H. B. Hartanto,^b M. Kraus,^c T. Weber^d and M. Worek^d

^a*MTA-DE Particle Physics Research Group, University of Debrecen, H-4010 Debrecen, PBox 105, Hungary*

^b*Institute for Particle Physics Phenomenology, Department of Physics, Durham University, Durham, DH1 3LE, UK*

^c*Humboldt-Universität zu Berlin, Institut für Physik, Newtonstraße 15, D-12489 Berlin, Germany*

^d*Institute for Theoretical Particle Physics and Cosmology, RWTH Aachen University, D-52056 Aachen, Germany*

E-mail:

giuseppe.bevilacqua@science.unideb.hu,

heribertus.b.hartanto@durham.ac.uk,

manfred.kraus@physik.hu-berlin.de,

tweber@physik.rwth-aachen.de,

worek@physik.rwth-aachen.de

ABSTRACT: With the goal of increasing the precision of NLO QCD predictions for the $pp \rightarrow t\bar{t}\gamma$ process in the di-lepton top quark decay channel we present theoretical predictions for the $\mathcal{R} = \sigma_{t\bar{t}\gamma}/\sigma_{t\bar{t}}$ cross section ratio. Results for the latter together with various differential cross section ratios are given for the LHC with the Run II energy of $\sqrt{s} = 13$ TeV. Fully realistic NLO computations for $t\bar{t}$ and $t\bar{t}\gamma$ production are employed. They are based on matrix elements for $e^+\nu_e\mu^-\bar{\nu}_\mu b\bar{b}$ and $e^+\nu_e\mu^-\bar{\nu}_\mu b\bar{b}\gamma$ processes and include all resonant and non-resonant diagrams, interferences, and off-shell effects of the top quarks and the W gauge bosons. Various renormalisation and factorisation scale choices and parton density functions are examined to assess their impact on the cross section ratio. Depending on the transverse momentum cut on the hard photon a judicious choice of a dynamical scale allows us to obtain 1% – 3% percent precision on \mathcal{R} . Moreover, for differential cross section ratios theoretical uncertainties in the range of 1% – 6% have been estimated. Until now such high precision predictions have only been reserved for the top quark pair production at NNLO QCD. Thus, \mathcal{R} at NLO in QCD represents a very precise observable to be measured at the LHC for example to study the top quark charge asymmetry or to probe the strength and the structure of the $t\bar{t}\gamma$ vertex. The latter can shed some light on possible new physics that can reveal itself only once sufficiently precise theoretical predictions are available.

KEYWORDS: NLO Computations, QCD Phenomenology, Heavy Quark Physics

TTK-18-20, HU-EP-18/26, IPPP/18/77

Contents

1	Introduction	1
2	Computational Framework and Input Parameters	4
3	Differential Cross Sections at NLO in QCD	6
4	Absolute Cross Sections at NLO in QCD	10
5	Cross Section Ratios at NLO in QCD	13
6	Differential Cross Section Ratios at NLO in QCD	17
7	Conclusions	22

1 Introduction

Top quark studies, that are currently driven by the Large Hadron Collider (LHC) experiments ATLAS and CMS, play a major role in deciphering the fundamental interactions. At the LHC top quarks are mostly produced in pairs through strong interactions, but they can also be created individually in single-top production via electroweak interactions. Thus, depending on the production mode, the top quark allows for different tests of the underlying forces. Both experiments concentrate on the measurements of top quark properties like for example the top quark mass (m_t), the top quark width (Γ_t), the top quark charge (Q_t), the total and differential cross sections as well as the top quark spin correlations and the top quark charge asymmetry (A_{tt}^C), including differential top quark charge asymmetries. High in the LHC program is the determination of the top quark couplings to gauge bosons and the Standard Model (SM) Higgs boson. Due to the large top quark mass various new physics scenarios introduce modifications within the top quark sector. Some examples include heavy new particles decaying into top quark pairs, flavour changing neutral currents, anomalous missing transverse momentum, same-sign top pair production or charged Higgs production. Such new physics models can be tested by precise measurements of top quark pairs, that are abundantly produced at the LHC. Furthermore, top quark production, also with additional b - or light jet(s), constitutes dominant irreducible backgrounds to many of the searches for new physics processes. Thus, it is vital to understand the properties and the characteristics of top production and decay mechanisms. The level of precision available on the theory side can have a huge impact on whether we can actually see the effects of new physics.

As a result of the large collision energy at the LHC also more exclusive final states, like for example $t\bar{t}\gamma$, have started to be accessible [1–3]. Even though the cross section for the $t\bar{t}\gamma$ production process at the LHC is much smaller than the cross section for the production of the top quark pair alone, the former can provide key information on the strength and the structure of the top quark coupling to the photon. Thus, it can for example substantially constrain anomalous top quark couplings at the LHC, see e.g. Ref. [4, 5]. Regardless of the

applications, whether these are measurements within the SM or outside of this framework, precise theoretical predictions are compulsory to carry out such measurements.

To increase the theoretical precision for $pp \rightarrow t\bar{t}\gamma$ higher order corrections in QCD should be consistently included. Moreover, the most accurate description of top quark decay chains has to be incorporated. Appropriate calculations have recently been made available. Specifically, a complete description of top quark pair production in association with a hard photon in the di-lepton top quark decay channel has been provided in Ref. [6]. The calculations include factorisable and non-factorisable contributions at NLO in QCD, that imply a cross talk between production and decays of top quarks which require going beyond the so-called Narrow Width Approximation (NWA). Specifically, they include double resonant, single resonant and non-resonant Feynman diagrams with respect to the top quark and W gauge boson, interferences among them as well as finite-width effects of t and W . With a fairly inclusive selection of cuts on the final states, which are two b -jets, a hard photon, two charged leptons and the missing transverse momentum, p_T^{miss} , the full pp cross section for a fixed renormalisation and factorisation scale choice receives negative and moderate NLO QCD corrections of 10%. An assessment of the uncertainties of theoretical origin left us with a 14% theoretical error. Inclusion of a kinematic dependent scale, that captures some parts of the unknown higher order effects, has improved the situation yielding positive and small NLO corrections of 2.5%. In this case the theoretical uncertainties resulting from scale variations have been estimated at the level of 6% only. The impact of higher order corrections on differential distributions, however, is much larger. For some observables, incidentally important in searches for new physics, shape distortions of more than 100% have been observed. As expected for specific phase space regions also the theoretical errors have increased substantially. Improvement of the accuracy of theoretical predictions also at the differential level to a few percent can be obtained by including the next order in the perturbative expansion in α_s . However, going beyond NLO even for on-shell $t\bar{t}\gamma$ production seems to be a formidable task at present. Inclusion of non-factorisable QCD contributions at NNLO is simply difficult to imagine. Instead, a ratio of cross sections can be studied since it may be significantly more stable against radiative corrections and scale variations than the cross sections themselves. Moreover, a ratio may reduce other theoretical uncertainties like for example those stemming from parton distribution functions. To this end a process that is under excellent theoretical control must be employed in the denominator of the ratio. The $t\bar{t}$ production process, albeit in the same decay channel, seems to be the best candidate for the job due to its large cross section and similar behaviour with regard to radiative corrections [7–9]. Consequently, the following cross section ratio

$$\mathcal{R} = \frac{\sigma_{t\bar{t}\gamma}}{\sigma_{t\bar{t}}}, \quad (1.1)$$

represents an interesting quantity to search for deviations from the SM theory at the LHC. Moreover, a set of differential cross section ratios can be constructed to look for any shape deviations from those predicted within the SM

$$\mathcal{R}_X = \left(\frac{d\sigma_{t\bar{t}\gamma}}{dX} \right) \left(\frac{d\sigma_{t\bar{t}}}{dX} \right)^{-1}. \quad (1.2)$$

Here X stands for the particular observable under consideration, e.g. the invariant mass of two charged leptons, $m_{\ell\ell}$, the invariant mass of two b -jets, $m_{b\bar{b}}$, etc. Since for a realistic analysis specific cuts on top quark decay products need to be imposed, a reliable description of top quark decays is mandatory for both processes $pp \rightarrow t\bar{t}\gamma$ and $pp \rightarrow t\bar{t}$. In order to avoid the introduction of additional unnecessary theoretical uncertainties to the construction of the cross section ratio, the same level of accuracy in the modelling of top quark decays must to be employed in the numerator and denominator of \mathcal{R} and \mathcal{R}_X . Besides the modelling of top quark decays, where the incorporation of radiative corrections is mandatory, a proper renormalisation and factorisation scale choice has to be carefully investigated. The scale choice should play an even greater role when various differential cross section ratios are constructed. For the latter phase space regions away from those dominated by double resonant top quark contributions, which are sensitive to non-factorizable QCD corrections, would be probed as well.

The purpose of this paper is twofold. First, we would like to provide a systematic analysis of the two processes $pp \rightarrow t\bar{t}\gamma$ and $pp \rightarrow t\bar{t}$ in the di-lepton top quark decay channel and extract the most accurate NLO prediction for the total cross section ratio. Such precise theoretical results can be used in comparisons with the LHC data. The second goal of the paper is to examine whether differential cross section ratios have enhanced predictive power for new physics searches, by investigating possible correlations between the two processes in various phase space regions in the quest of reducing theoretical errors. Calculations for both processes will be carried out with the same input parameters, parton distribution functions (PDFs), jet algorithm and the same set of inclusive cuts up to the cuts on the hard photon, which are present only in the case of $t\bar{t}\gamma$ production. Finally, for both processes factorisation and renormalisation scales will be set to a common fixed value, whereas for a dynamical scale choice scales as similar as possible will be selected. Cross section ratios calculated in this way are free of additional and undesired theoretical uncertainties that are introduced when different input parameters are employed in the numerator and the denominator of \mathcal{R} . The size of such additional theoretical uncertainties, however, must be estimated. In various experimental analyses different Monte Carlo (MC) programs are employed to provide theoretical predictions for $t\bar{t}$ and $t\bar{t}\gamma$ production. Such general purpose MC frameworks are often used by experimental collaborations with a default set up, among others with a different scale choice and parton distribution functions for $pp \rightarrow t\bar{t}$ and $pp \rightarrow t\bar{t}\gamma$. Thus, in the paper we will quantify the impact of the additional theoretical uncertainties coming from different theoretical inputs. Finally, the stability of the cross section ratio with respect to the transverse momentum cut on the hard photon will be examined. To this end, theoretical predictions for $t\bar{t}\gamma$ production will be evaluated for two different values of the $p_{T,\gamma}$ cut.

The article is organised as follows. In Section 2 the HELAC-NLO computational framework and input parameters used in our studies are described. In Section 3 the normalised differential cross sections for off-shell $t\bar{t}\gamma$ and $t\bar{t}$ production are provided in order to study the correlation of the two processes. The results given there are used to understand how the theoretical errors on the cross section ratios should be estimated. NLO predictions for absolute cross sections are presented in Section 4 together with the theoretical uncertainties

from the scale dependence. Additionally, results with different parton distribution functions are shown in Section 4. They are calculated to estimate the size of theoretical uncertainties that come from the parametrisation of parton distribution functions. In Section 5 we provide results for NLO cross section ratios. Theoretical uncertainties are also discussed there. Theoretical predictions for the differential cross section ratios and their theoretical uncertainties are exhibited and discussed in Section 6. Finally, in Section 7 our conclusions are laid out.

2 Computational Framework and Input Parameters

All the LO and NLO results for $e^+\nu_e\mu^-\bar{\nu}_\mu b\bar{b}\gamma$ and $e^+\nu_e\mu^-\bar{\nu}_\mu b\bar{b}$ production, which are presented in this paper, have been obtained with the help of the HELAC-NLO MC framework [10]. The package comprises HELAC-1LOOP [11] with CUTTOOLS [12] for the virtual corrections and HELAC-DIPOLES [13, 14] for the real emission part. The HELAC-DIPOLES software deals with singularities from soft or collinear parton emissions that are isolated via subtraction methods for NLO QCD calculations. Specifically, the commonly used Catani-Seymour dipole subtraction [13, 15, 16] and the so-called Nagy-Soper subtraction scheme [14] are both implemented in the HELAC-DIPOLES program and used in our simulations. The integration over the phase space has been achieved with the help of KALEU [17]. For unstable top quarks the complex mass scheme is utilised [18, 19]. At the one loop level the appearance of $\Gamma_t \neq 0$ in the propagator requires the evaluation of scalar integrals with complex masses, which is supported by the ONELOOP program [20]. Further details of these calculations can be found in our earlier work on $pp \rightarrow t\bar{t}$ [8], $pp \rightarrow t\bar{t}j$ [21, 22] and $pp \rightarrow t\bar{t}\gamma$ [6] where complete top quark off-shell effects have also been consistently taken into account at the NLO level in QCD. Specifically, in each case all resonant and non-resonant Feynman diagrams, interferences and finite width effects of the top quark as well as W gauge bosons have been included. The methods developed there have been straightforwardly adapted in the current studies and, therefore, do not need a recollection. We refer the interested readers to previously published results. In the calculations of cross sections for $e^+\nu_e\mu^-\bar{\nu}_\mu b\bar{b}\gamma$ and $e^+\nu_e\mu^-\bar{\nu}_\mu b\bar{b}$ we employ the following SM parameters

$$\begin{aligned}
G_F &= 1.166378 \cdot 10^{-5} \text{ GeV}^{-2}, & m_t &= 173.2 \text{ GeV}, \\
m_W &= 80.385 \text{ GeV}, & \Gamma_W &= 2.0988 \text{ GeV}, \\
m_Z &= 91.1876 \text{ GeV}, & \Gamma_Z &= 2.50782 \text{ GeV}, \\
\Gamma_t^{\text{LO}} &= 1.47848 \text{ GeV}, & \Gamma_t^{\text{NLO}} &= 1.35159 \text{ GeV}.
\end{aligned}
\tag{2.1}$$

All other particles including bottom quarks are treated as massless. Since leptonic W gauge boson decays do not receive NLO QCD corrections, to account for some higher order effects the NLO QCD values for the gauge boson widths are used everywhere, i.e. for LO and NLO matrix elements. The electromagnetic coupling α is calculated from the Fermi constant G_F in the G_μ -scheme via

$$\alpha_{G_\mu} = \frac{\sqrt{2}}{\pi} G_F m_W^2 \left(1 - \frac{m_W^2}{m_Z^2} \right).
\tag{2.2}$$

For the emission of the isolated photon, however, $\alpha_{\text{QED}} = 1/137$ is used instead. The running of the strong coupling constant α_s with two-loop (one-loop) accuracy at NLO (LO) is provided by the LHAPDF interface [23]. The number of active flavours is set to $N_F = 5$, however, contributions induced by the bottom-quark parton density are neglected due to their numerical insignificance. Following recommendations of PDF4LHC [24] for the usage of parton distribution functions (PDFs) suitable for applications at the LHC Run II we employ CT14 [25], which is our default choice, MMHT14 [26] and NNPDF3.0 [27] PDFs. Our calculation, like any fixed-order calculations, contains a residual dependence on the renormalisation (μ_R) and the factorisation scales (μ_F) arising from the truncation of the perturbative expansion in α_s . As a consequence, all observables depend on the values of μ_R and μ_F that are provided as input parameters. The theoretical uncertainty of the total cross section, associated with neglected higher order terms in the perturbative expansion, can be estimated by varying μ_R and μ_F in α_s and in the PDFs. We assume that μ_R and μ_F are set to a common value $\mu_R = \mu_F = \mu_0$. However, the scale dependence is evaluated by varying μ_R and μ_F independently in the range

$$\frac{1}{2} \mu_0 \leq \mu_R, \mu_F \leq 2 \mu_0, \quad (2.3)$$

with the additional condition

$$\frac{1}{2} \leq \frac{\mu_R}{\mu_F} \leq 2. \quad (2.4)$$

In practice, such restrictions are equivalent to evaluating the following scale variations

$$\left(\frac{\mu_R}{\mu_0}, \frac{\mu_F}{\mu_0} \right) = \{(2, 1), (0.5, 1), (1, 2), (1, 1), (1, 0.5), (2, 2), (0.5, 0.5)\}. \quad (2.5)$$

The final error is estimated from the envelope of the resulting cross sections. For the central value of the scale, μ_0 , we consider the fixed scale (the phase-space independent scale choice) $\mu_0 = m_t/2$ and the dynamic scale (the phase-space dependent scale choice) $\mu_0 = H_T/4$. The latter is defined on an event-by-event basis according to

$$H_T = p_{T,e^+} + p_{T,\mu^-} + p_T^{miss} + p_{T,b_1} + p_{T,b_2}, \quad (2.6)$$

where p_T^{miss} denotes missing transverse momentum and p_{T,b_1}, p_{T,b_2} are transverse momenta of the two b -jets. In the case of $pp \rightarrow t\bar{t}\gamma$ the transverse momentum of the hard photon is also included into the definition of H_T . Jets are constructed from final-state partons with pseudo-rapidity $|\eta| < 5$ with the help of the infrared safe *anti- k_T* jet algorithm [28] with the separation parameter $R = 0.4$. For $e^+\nu_e\mu^-\bar{\nu}_\mu b\bar{b}$ production exactly two b -jets, two charged leptons and missing transverse momentum are required. Additionally, for the $e^+\nu_e\mu^-\bar{\nu}_\mu b\bar{b}\gamma$ production process an isolated hard photon is requested. The latter is defined with $p_{T,\gamma} > 25$ GeV (our default transverse momentum cut on the hard photon) and $|y_\gamma| < 2.5$ [2, 3]. To examine the stability of our theoretical predictions at NLO in QCD we also present results for the higher value of the $p_{T,\gamma}$ cut, namely for $p_{T,\gamma} > 50$ GeV. To ensure infrared safety we use the photon isolation prescription described in Ref. [29] that is based on a modified cone approach. The photon isolation condition is implemented

in the same way for quarks and gluons. For each parton i we evaluate the distance in the rapidity-azimuthal angle plane between this parton and the photon, according to

$$\Delta R_{\gamma i} = \sqrt{\Delta y_{\gamma i}^2 + \Delta \phi_{\gamma i}^2} = \sqrt{(y_\gamma - y_i)^2 + (\phi_\gamma - \phi_i)^2}. \quad (2.7)$$

We reject the event unless the following condition is fulfilled

$$\sum_i E_{T,i} \Theta(R - R_{\gamma i}) \leq E_{T,\gamma} \left(\frac{1 - \cos(R)}{1 - \cos(R_{\gamma j})} \right), \quad (2.8)$$

where $R \leq R_{\gamma j} = 0.4$ and i runs over all partons. Moreover, $E_{T,i}$ is the transverse energy of the parton i and $E_{T,\gamma}$ is the transverse energy of the photon. We apply all other selection criteria to jets if and only if their separation from the photon exceeds $R_{\gamma j}$. A jet reconstructed inside the cone size $R_{\gamma j}$ is not subjected to any cuts. All final states have to fulfil the subsequent selection criteria that mimic as closely as possible the ATLAS and the CMS detector acceptances [2, 3]

$$\begin{array}{lll} p_{T,\ell} > 30 \text{ GeV} & p_{T,b} > 40 \text{ GeV} & p_T^{miss} > 20 \text{ GeV} \\ |y_\ell| < 2.5 & |y_b| < 2.5 & \Delta R_{\ell\gamma} > 0.4 \\ \Delta R_{\ell b} > 0.4 & \Delta R_{bb} > 0.4 & \Delta R_{\ell\ell} > 0.4. \end{array} \quad (2.9)$$

We set no restriction on the kinematics of the extra (non b -)jet.

3 Differential Cross Sections at NLO in QCD

In this Section we present results for differential cross section distributions for both processes: $pp \rightarrow e^+ \nu_e \mu^- \bar{\nu}_\mu b\bar{b} \gamma + X$ at $\mathcal{O}(\alpha_s^3 \alpha^5)$ and $pp \rightarrow e^+ \nu_e \mu^- \bar{\nu}_\mu b\bar{b} + X$ at $\mathcal{O}(\alpha_s^3 \alpha^4)$. They are obtained for the LHC Run II energy of $\sqrt{s} = 13$ TeV. For brevity, we will refer to these reactions as $pp \rightarrow t\bar{t}\gamma$ and $pp \rightarrow t\bar{t}$. To understand similarities and potential differences between the two production processes, it is helpful to identify the dominant partonic subprocesses. In both cases the most important production mechanism is via scattering of two gluons. With our selection of cuts, the gg channel contributes 79% (88%) to the LO $pp \rightarrow t\bar{t}\gamma$ ($pp \rightarrow t\bar{t}$) cross section while the $q\bar{q} + \bar{q}q$ channels account for 21% (12%). The dominance of the gg production process in both cases suggests that $pp \rightarrow t\bar{t}$ and $pp \rightarrow t\bar{t}\gamma$ should show similar features in the kinematics of the final states, i.e. two charged leptons, the missing transverse momentum and two b -jets. All differential cross sections that are presented in the following have been obtained for the CT14 PDF set. For both production processes we use the kinematic-independent factorisation and renormalisation scales $\mu_R = \mu_F = \mu_0$ with the central value $\mu_0 = m_t/2$ rather than simply $\mu_0 = m_t$. Even though the mass of the heaviest particle appearing in the process seems to be a more natural option, the $\mu_0 = m_t/2$ scale choice is very well motivated by the fact that $pp \rightarrow t\bar{t}$ at the LHC is dominated by t -channel gluon fusion, which favours smaller values of the scale. Additionally, effects beyond NLO that include soft-gluon resummation for the hadronic cross-section at next-to-leading logarithmic accuracy are smaller for $\mu_0 = m_t/2$ than for $\mu_0 = m_t$ [30, 31]

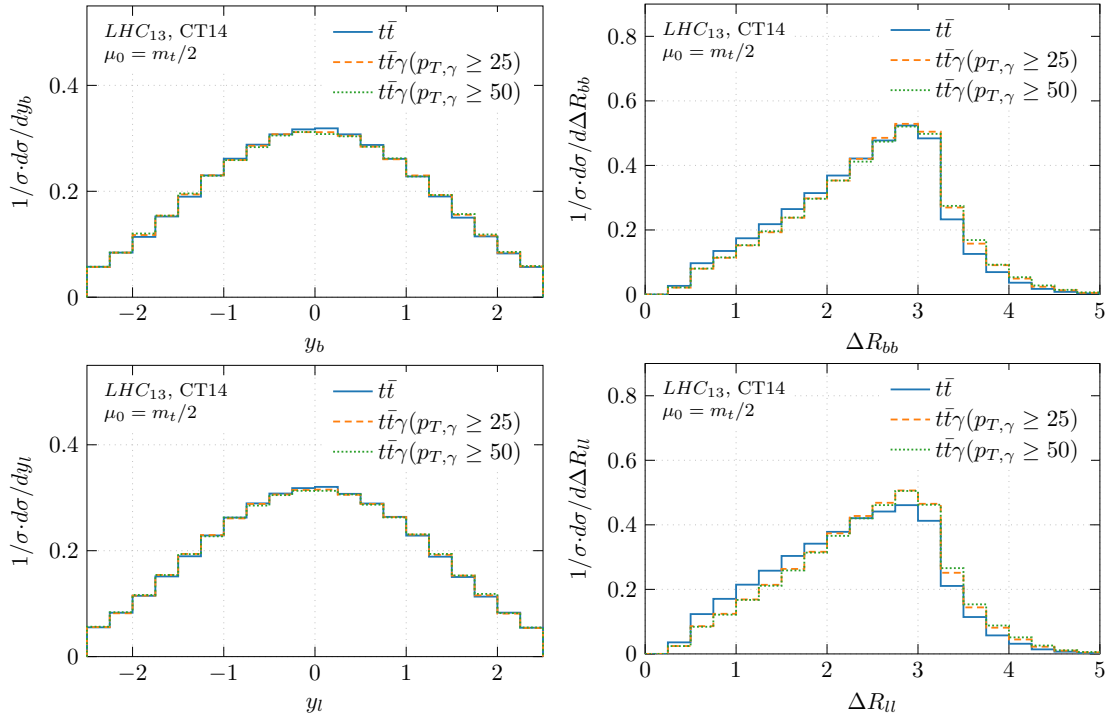


Figure 1. Comparison of the normalised NLO differential cross sections for $pp \rightarrow e^+ \nu_e \mu^- \bar{\nu}_\mu b \bar{b} \gamma + X$ and $pp \rightarrow e^+ \nu_e \mu^- \bar{\nu}_\mu b \bar{b} + X$ at the LHC with $\sqrt{s} = 13$ TeV. We present: the averaged rapidity of the b -jet (y_b), the distance in the azimuthal angle rapidity plane between two b -jets (ΔR_{bb}), the averaged rapidity of the charged lepton (y_ℓ) as well as the distance in the azimuthal angle rapidity plane between two charged leptons ($\Delta R_{\ell\ell}$). Results for two different values of the transverse momentum cut on the hard photon are shown. The NLO CT14 PDF set is employed and $\mu_R = \mu_F = \mu_0 = m_t/2$ is used.

as we have explicitly checked with the help of the TOP++ program [32]. From the QCD point of view both processes $pp \rightarrow t\bar{t}$ and $pp \rightarrow t\bar{t}\gamma$ are similar, which motivates our scale choice for $pp \rightarrow t\bar{t}\gamma$ as well.

We start with a collection of angular cross section distributions that are given in Figure 1. Specifically, we present the averaged rapidity distribution of the b -jet and the charged lepton as well as the separation in the rapidity-azimuthal angle plane between the two b -jets, ΔR_{bb} , and between the two charged leptons, $\Delta R_{\ell\ell}$. All differential cross section distributions are normalised to the corresponding absolute cross sections to illustrate shape similarities and differences between the two processes. For the $pp \rightarrow t\bar{t}$ process the two b -jets are emitted in the central regions (in rapidity) of the detector. This is a consequence of the dominance of the gg production channel, which favours emissions of jets at smaller rapidities. Charged leptons are also produced mostly centrally. Moreover, both charged leptons ℓ^\pm and b -jets are preferably produced in the back-to-back configurations. Hereby, b -jets come more often from top quark decays rather than from the $g \rightarrow b\bar{b}$ splitting. The latter configuration would manifest itself in the enhancement in the lower values of ΔR_{bb} .

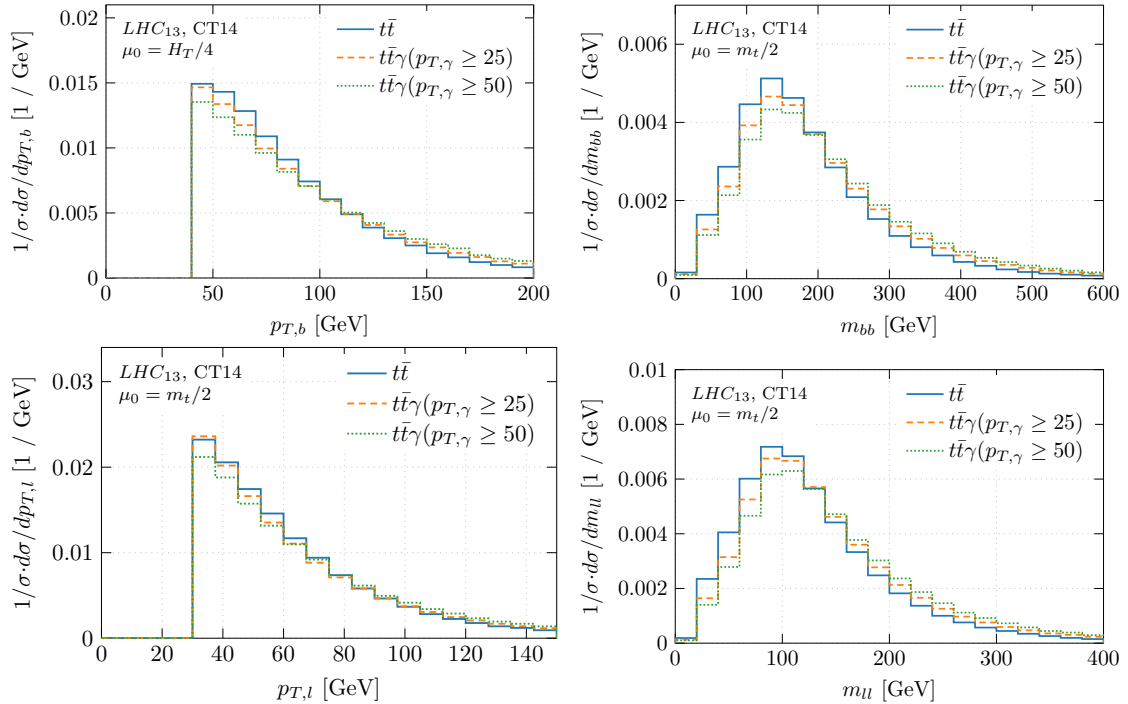


Figure 2. Comparison of the normalised NLO differential cross sections for $pp \rightarrow e^+ \nu_e \mu^- \bar{\nu}_\mu b \bar{b} \gamma + X$ and $pp \rightarrow e^+ \nu_e \mu^- \bar{\nu}_\mu b \bar{b} + X$ at the LHC with $\sqrt{s} = 13$ TeV. The following distributions are shown: the averaged transverse momentum of the b -jet ($p_{T,b}$), the invariant mass of two b -jets ($m_{b\bar{b}}$), the averaged transverse momentum of the charged lepton ($p_{T,\ell}$) and the invariant mass of two charged leptons ($m_{\ell\bar{\ell}}$). Results for two different values of the transverse momentum cut on the hard photon are shown. The NLO CT14 PDF set is employed and $\mu_R = \mu_F = \mu_0 = m_t/2$ is used.

Singularities stemming from the collinear $g \rightarrow b\bar{b}$ splitting are, however, screened off by the (effective) invariant mass cut of $m_{b\bar{b}} \gtrsim 16$ GeV. The latter is implied once the $\Delta R_{b\bar{b}}$ separation between the two b -jets of 0.4 is introduced by the jet algorithm together with the requirement of having both b -jets with transverse momentum larger than 40 GeV. For the two charged leptons the situation is rather simplified due to the fact that we simulate decays of the weak bosons to different lepton generations only, thus, virtual photon singularities stemming from collinear $\gamma \rightarrow \ell^+ \ell^-$ decays are avoided. As might be observed in Figure 1 we can not see large shape differences in dimensionless observables, when the emission of the additional hard photon is included. This is in line with our expectation that the $t\bar{t}$ and $t\bar{t}\gamma$ production processes are similar from the QCD point of view. All the kinematical features described above are insensitive to the $p_{T,\gamma}$ cut as can be additionally observed in Figure 1 since results for two cases $p_{T,\gamma} > 25$ GeV and $p_{T,\gamma} > 50$ GeV are plotted.

In the next step, we consider dimensionful observables like for example the averaged transverse momentum of the b -jet, the averaged transverse momentum of the charged lepton as well as the invariant mass of the two charged leptons and the two b -jets. They are collected in Figure 2. Again shapes of all observables are not affected by the hard photon

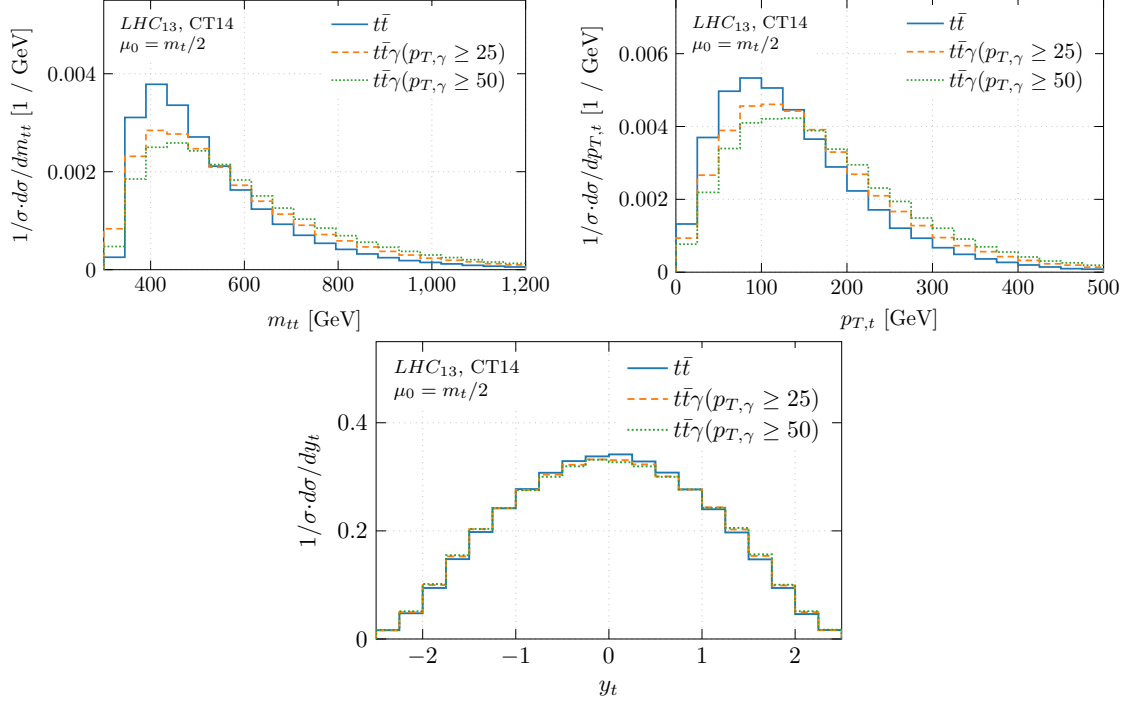


Figure 3. Comparison of the normalised NLO differential cross sections for $pp \rightarrow e^+ \nu_e \mu^- \bar{\nu}_\mu \bar{b}\bar{b} \gamma + X$ and $pp \rightarrow e^+ \nu_e \mu^- \bar{\nu}_\mu \bar{b}\bar{b} + X$ at the LHC with $\sqrt{s} = 13$ TeV. The top quark kinematics is shown. Specifically, the invariant mass of the reconstructed $t\bar{t}$ system ($m_{t\bar{t}}$) as well as the averaged transverse momentum ($p_{T,t}$) and rapidity (y_t) of the top quark are depicted. Results for two different values of the transverse momentum cut on the hard photon are shown. The NLO CT14 PDF set is employed and $\mu_R = \mu_F = \mu_0 = m_t/2$ is used.

emissions. In the case of $pp \rightarrow t\bar{t}\gamma$ all plotted spectra are slightly harder. However, this is a consequence of the additional $p_{T,\gamma}$ cut that effectively sets higher transverse momentum thresholds on the whole $t\bar{t}$ system, thus, consequently on all top quark decay products. Overall, for $t\bar{t}$ and $t\bar{t}\gamma$ production similarities in the jet activity and the way charged leptons are produced could be observed.

Subsequently, we turn our attention to the common underlying $t\bar{t}$ kinematics. To this end, in Figure 3 we depict the invariant mass of the $t\bar{t}$ system as well as the averaged transverse momentum and rapidity of the top quark. We note here, that top quarks are reconstructed from their decay products assuming exact reconstruction of the W gauge boson. Specifically, we have defined $p(t) = p(b) + p(e^+) + p(\nu_e)$ and $p(\bar{t}) = p(\bar{b}) + p(\mu^-) + p(\bar{\nu}_\mu)$, where b and \bar{b} denotes the b -jets. We could observe harder spectra for the averaged transverse momentum of the top quark and for the invariant mass of the $t\bar{t}$ system in the case of the $t\bar{t}\gamma$ production process as compared to the corresponding distributions for $t\bar{t}$ production. Since we consider the whole reconstructed top quark system, not only its decay products separately, the higher transverse momentum threshold set by the $p_{T,\gamma}$ cut is more pronounced here. Moreover, for both processes the top quarks are predominantly produced in the central rapidity regions and in the back-to-back configuration.

PDF set, $\mu_R = \mu_F = \mu_0$	$\sigma_{e^+\nu_e\mu^-\bar{\nu}_\mu b\bar{b}}^{\text{NLO}}$ [fb]	$\sigma_{e^+\nu_e\mu^-\bar{\nu}_\mu b\bar{b}\gamma}^{\text{NLO}}$ [fb]	$\sigma_{e^+\nu_e\mu^-\bar{\nu}_\mu b\bar{b}\gamma}^{\text{NLO}}$ [fb]
		$p_{T,\gamma} > 25$ GeV	$p_{T,\gamma} > 50$ GeV
CT14, $\mu_0 = m_t/2$	$1629.4^{+18.4(1\%)}_{-144.7(9\%)}$	$7.436^{+0.074(1\%)}_{-1.034(14\%)}$	$3.081^{+0.050(2\%)}_{-0.514(17\%)}$
CT14, $\mu_0 = H_T/4$	$1620.5^{+21.6(1\%)}_{-118.8(7\%)}$	$7.496^{+0.099(1\%)}_{-0.457(6\%)}$	$3.125^{+0.040(1\%)}_{-0.142(4\%)}$
MMHT14, $\mu_0 = m_t/2$	$1650.5^{+17.0(1\%)}_{-152.7(9\%)}$	$7.490^{+0.080(1\%)}_{-1.081(14\%)}$	$3.093^{+0.053(2\%)}_{-0.535(17\%)}$
NNPDF3.0, $\mu_0 = m_t/2$	$1695.0^{+18.4(1\%)}_{-153.3(9\%)}$	$7.718^{+0.078(1\%)}_{-1.102(14\%)}$	$3.195^{+0.054(2\%)}_{-0.550(17\%)}$

Table 1. *NLO cross sections for $pp \rightarrow e^+\nu_e\mu^-\bar{\nu}_\mu b\bar{b} + X$ and $pp \rightarrow e^+\nu_e\mu^-\bar{\nu}_\mu b\bar{b}\gamma + X$ at the LHC with $\sqrt{s} = 13$ TeV. Also included are theoretical errors as obtained from the scale variation. In the case of $pp \rightarrow e^+\nu_e\mu^-\bar{\nu}_\mu b\bar{b}\gamma + X$ results for two different values of the $p_{T,\gamma}$ cut are given. Various PDF sets are employed.*

To summarise this part, let us repeat that as anticipated both $t\bar{t}\gamma$ and $t\bar{t}$ production processes are highly correlated. This fact will be exploited in the next section when the theoretical error for the $t\bar{t}\gamma$ and $t\bar{t}$ cross section ratio will be estimated. Additionally, conclusions drawn here are independent of the $p_{T,\gamma}$ cut. Furthermore, they are not modified when the dynamical scale choice ($\mu_R = \mu_F = \mu_0 = H_T/4$) is used instead for both processes or when different PDF sets (MMHT14 or NNPDF3.0) are employed.

4 Absolute Cross Sections at NLO in QCD

In this Section we present predictions for $pp \rightarrow e^+\nu_e\mu^-\bar{\nu}_\mu b\bar{b}$ and $pp \rightarrow e^+\nu_e\mu^-\bar{\nu}_\mu b\bar{b}\gamma$ at the LHC with $\sqrt{s} = 13$ TeV. NLO QCD cross sections are shown in Table 1 together with their theoretical errors from the scale dependence. Results are presented for the following two values of the transverse momentum cut on the hard photon $p_{T,\gamma} > 25$ GeV and $p_{T,\gamma} > 50$ GeV. The default CT14 PDF set is employed together with two additional PDF sets, namely MMHT14 and NNPDF3.0. Moreover, the following two scale choices, $\mu_0 = m_t/2$ and $\mu_0 = H_T/4$, are studied. In the first step we examine results that we have obtained for the CT14 PDF set. Looking at the total cross sections, which are mostly influenced by final state production relatively close to the $t\bar{t}$ threshold, both scale choices are in equally good shape since the results agree well within the corresponding theoretical errors. However, the size of the theoretical uncertainties, especially in the case of $t\bar{t}\gamma$ production, does depend on the scale choice. The latter finding tells us that the absolute cross sections for $t\bar{t}$ and $t\bar{t}\gamma$ production in the di-lepton top quark decay channel with the selection of cuts that we have imposed are not as inclusive observables as one would expect. Specifically, for $\mu_0 = m_t/2$ the NLO theoretical uncertainties for the $pp \rightarrow t\bar{t}\gamma$ process are of the order of 14% for $p_{T,\gamma} > 25$ GeV and 17% for $p_{T,\gamma} > 50$ GeV. In the case of $t\bar{t}$

production theoretical uncertainties, as obtained from Eq. (2.5), of the order of 9% have been estimated. For the dynamical scale choice in each case the theoretical uncertainties are well below 10%. Specifically, our judicious dynamical scale choice has allowed us to obtain 7% for $t\bar{t}$ production and 6% for $t\bar{t}\gamma$ production with $p_{T,\gamma} > 25$ GeV. In the latter case an increase of the transverse momentum cut to 50 GeV has resulted in the smaller theoretical error of 4%. These facts suggest that the proposed dynamical scale efficiently describes the multi-scale kinematics of the process. Let us note at this point, that should we instead vary μ_R and μ_F simultaneously, up and down by a factor of 2 around μ_0 , the uncertainties would remain unchanged. This is due to the fact that the scale variation is driven solely by the changes in μ_R , see Ref. [6].

Before discussing results for other PDF sets let us remind the reader in this place that in the case of on-shell $t\bar{t}$ and $t\bar{t}\gamma$ production for stable top quarks the size of the theoretical error as obtained from the scale dependence is not substantially reduced when the dynamical scale choice is used instead of the fixed one, of course as long as this scale is properly selected. To better outline this conclusion, we show the NLO QCD results for on-shell $t\bar{t}$ and $t\bar{t}\gamma$ production at the LHC, that we denote with a special index “(on-shell)” to distinguish them from the results with top quark and W gauge boson decays and off-shell effects included. Results are generated with the same input parameters as given in Section 2. For the on-shell $t\bar{t}$ sample we do not apply any kinematical cuts, while in the case of $t\bar{t}\gamma$ we apply cuts on the hard photon only, following the same criteria used for the off-shell case. Namely, we ask for $p_{T,\gamma} > 25$ GeV, $|y_\gamma| < 2.5$ and $R_{\gamma j} = 0.4$ in the photon isolation condition. In the LO-like configurations the latter condition is translated to the simpler $\Delta R_{\gamma j} > 0.4$ cut where j stands for all light partons including bottom quarks. Additionally, we present these results for the following two scale choices $\mu_R = \mu_F = \mu_0 = m_t/2$ and $\mu_R = \mu_F = \mu_0 = E_T/4$. The dynamical scale choice, which is defined as

$$E_T = \sqrt{p_T^2(t) + m_t^2} + \sqrt{p_T^2(\bar{t}) + m_t^2}, \quad (4.1)$$

is similar to our previous choice $\mu_0 = H_T/4$ ¹. For obvious reasons the latter can not be applied for the on-shell $t\bar{t}$ and $t\bar{t}\gamma$ production. Once more in the case of $pp \rightarrow t\bar{t}\gamma$ the transverse momentum of the hard photon, $p_{T,\gamma}$, has been added to the definition of E_T . Our results for top quark pair production can be summed up as

$$\begin{aligned} \sigma_{t\bar{t}}^{\text{NLO (on-shell)}}(\mu_0 = m_t/2, \text{CT14}) &= 797.07_{-82.41}^{+65.88} \text{ (8\%)} \text{ pb}, \\ \sigma_{t\bar{t}}^{\text{NLO (on-shell)}}(\mu_0 = E_T/4, \text{CT14}) &= 770.11_{-83.92}^{+74.61} \text{ (10\%)} \text{ pb}. \end{aligned} \quad (4.3)$$

¹For example for $\mu_R = \mu_F = \mu_0$ set to $\mu_0 = E_T/4$ we have obtained the following results for $e^+\nu_e\mu^-\bar{\nu}_\mu b\bar{b}$ and $e^+\nu_e\mu^-\bar{\nu}_\mu b\bar{b}\gamma$ production

$$\begin{aligned} \sigma_{e^+\nu_e\mu^-\bar{\nu}_\mu b\bar{b}}^{\text{NLO}}(\mu_0 = E_T/4, \text{CT14}) &= 1628.4_{-69.9}^{+19.7} \text{ (1\%)} \text{ fb}, \\ \sigma_{e^+\nu_e\mu^-\bar{\nu}_\mu b\bar{b}\gamma}^{\text{NLO}}(\mu_0 = E_T/4, \text{CT14}) &= 7.524_{-0.393}^{+0.106} \text{ (1\%)} \text{ fb}. \end{aligned} \quad (4.2)$$

In the latter case the $p_{T,\gamma} > 25$ GeV cut has been applied on the hard photon.

For $pp \rightarrow t\bar{t}\gamma$, on the other hand, we have obtained

$$\begin{aligned}\sigma_{t\bar{t}\gamma}^{\text{NLO (on-shell)}}(\mu_0 = m_t/2, \text{CT14}, p_{T,\gamma} > 25 \text{ GeV}) &= 2.035_{-0.211}^{+0.137} \text{ (7\%)} \text{ pb}, \\ \sigma_{t\bar{t}\gamma}^{\text{NLO (on-shell)}}(\mu_0 = E_T/4, \text{CT14}, p_{T,\gamma} > 25 \text{ GeV}) &= 1.901_{-0.227}^{+0.209} \text{ (11\%)} \text{ pb}.\end{aligned}\tag{4.4}$$

The theoretical uncertainties for the on-shell $t\bar{t}$ and $t\bar{t}\gamma$ production process are at the level of 10% – 11% for $pp \rightarrow t\bar{t}$ and 10% – 12% for $pp \rightarrow t\bar{t}\gamma$.

The theoretical uncertainties as obtained from the scale dependence of the studied cross sections are, however, not the only source of systematic uncertainties. Another source of theoretical uncertainties is associated with the parameterisation of PDFs. Thus, we have given in Table 1 NLO results for two additional PDF sets MMHT14 and NNPDF3.0 for $\mu_0 = m_t/2$. In this way the various theoretical assumptions that enter into the parameterisation of the PDFs, which are difficult to quantify within a given scheme, are assessed. When comparing CT14 results for $\sigma_{t\bar{t}\gamma}^{\text{NLO}}$ and $\sigma_{t\bar{t}}^{\text{NLO}}$ with the corresponding numbers for MMHT14 and NNPDF3.0 we observe that the PDF uncertainties for NLO cross sections are of the order of 1% for MMHT14 for both production processes. In the case of the NNPDF3.0 set they are at the level of 4%. Taken very conservatively as the maximum of MMHT14 and NNPDF3.0 results PDF uncertainties for $t\bar{t}$ and $t\bar{t}\gamma$ are estimated to be of the order of 4%. We have also performed the individual estimates of PDF systematics. We have followed the prescription of each PDF collaboration in order to provide the 68% confidence level (C.L.) PDF uncertainties. Both CT14 and MMHT14 include a central set and error sets in the Hessian representation. More precisely, there are $2N = 56$ and $2N = 50$ eigenvector PDF members for CT14 and MMHT14 respectively that we have employed to the asymmetric expression for PDF uncertainties as described for example in Ref [23]. Let us note at this point that the CT14 errors are rescaled by a factor 1/1.645 since they are originally provided only at 90% C.L. On the other hand for the NNPDF3.0 PDF set, which uses the Monte Carlo sampling method in conjunction with neural networks, PDF uncertainties are obtained using the replicas method, see e.g. Ref [23]. In this case a set of $N = 100$ Monte Carlo PDF members has been used to extract PDF uncertainties from the the NNPDF3.0 PDF set. Our findings for the $e^+\nu_e\mu^-\bar{\nu}_\mu b\bar{b}\gamma$ production process can be summarised as follows

$$\begin{aligned}\sigma_{e^+\nu_e\mu^-\bar{\nu}_\mu b\bar{b}\gamma}^{\text{NLO}}(\mu_0 = m_t/2, \text{CT14}, p_{T,\gamma} > 25 \text{ GeV}) &= 7.436_{-0.235}^{+0.220} \text{ (3\%)} \text{ fb}, \\ \sigma_{e^+\nu_e\mu^-\bar{\nu}_\mu b\bar{b}\gamma}^{\text{NLO}}(\mu_0 = m_t/2, \text{MMHT14}, p_{T,\gamma} > 25 \text{ GeV}) &= 7.490_{-0.143}^{+0.160} \text{ (2\%)} \text{ fb}, \\ \sigma_{e^+\nu_e\mu^-\bar{\nu}_\mu b\bar{b}\gamma}^{\text{NLO}}(\mu_0 = m_t/2, \text{NNPDF3.0}, p_{T,\gamma} > 25 \text{ GeV}) &= 7.718 \pm 0.106 \text{ (1\%)} \text{ fb}.\end{aligned}\tag{4.5}$$

On the other hand for $e^+\nu_e\mu^-\bar{\nu}_\mu b\bar{b}$ production we have obtained

$$\begin{aligned}\sigma_{e^+\nu_e\mu^-\bar{\nu}_\mu b\bar{b}}^{\text{NLO}}(\mu_0 = m_t/2, \text{CT14}) &= 1629.4_{-49.3}^{+44.6} \text{ (3\%)} \text{ fb}, \\ \sigma_{e^+\nu_e\mu^-\bar{\nu}_\mu b\bar{b}}^{\text{NLO}}(\mu_0 = m_t/2, \text{MMHT14}) &= 1650.5_{-33.1}^{+35.1} \text{ (2\%)} \text{ fb}, \\ \sigma_{e^+\nu_e\mu^-\bar{\nu}_\mu b\bar{b}}^{\text{NLO}}(\mu_0 = m_t/2, \text{NNPDF3.0}) &= 1695.0 \pm 26.0 \text{ (1.5\%)} \text{ fb}.\end{aligned}\tag{4.6}$$

Overall, we can observe that the size of the (internal) PDF uncertainties for each PDF set separately is of the order of 1% – 3%, therefore, smaller than the difference between various PDF sets, which is at the level of 1% – 4%. Nevertheless, for the total $e^+\nu_e\mu^-\bar{\nu}_\mu b\bar{b}$ and $e^+\nu_e\mu^-\bar{\nu}_\mu b\bar{b}\gamma$ cross sections the PDF uncertainties are below the theoretical uncertainties due to scale dependence, which remain the dominant source of the theoretical systematics.

5 Cross Section Ratios at NLO in QCD

In the following, we study the cross section ratios. Our main goal here is to verify whether even further improvement in the accuracy of theoretical predictions can be obtained. More precisely we would like to see if theoretical uncertainties below 10% can be obtained for the fixed scale choice. On the other hand, in the case of the dynamical scale choice, that has been adopted for these studies, we would like to determine whether a few percent precision, i.e. comparable accuracy to that of NNLO calculations for $t\bar{t}$ production [33, 34], might be achieved. To this end results for $\mathcal{R} = \sigma_{t\bar{t}\gamma}/\sigma_{t\bar{t}}$ cross sections ratio for the $p_{T,\gamma}$ cut of $p_{T,\gamma} > 25$ GeV and $p_{T,\gamma} > 50$ GeV are provided. They are constructed with the help of the absolute cross sections that are collected in Table 1. The theoretical error for the cross section ratio is estimated by calculating

$$\mathcal{R} = \frac{\sigma_{t\bar{t}\gamma}^{\text{NLO}}(\mu_1)}{\sigma_{t\bar{t}}^{\text{NLO}}(\mu_2)}, \quad (5.1)$$

where $\mu_1 = \mu_2 = \mu_0$ and due to correlation of $pp \rightarrow t\bar{t}\gamma$ and $pp \rightarrow t\bar{t}$ only the following combinations are considered, see e.g. Ref. [35]

$$\left(\frac{\mu_1}{\mu_0}, \frac{\mu_2}{\mu_0}\right) = \{(2, 2), (0.5, 0.5)\}. \quad (5.2)$$

Specifically, we use values of cross sections from Table 1 also for the scale dependence. The latter have been estimated with the help of Eq. (2.5). Nevertheless, since the scale variation in total cross sections is driven solely by the changes in μ_R , see Ref. [6], this is equivalent to employing Eq. (5.2). For $p_{T,\gamma} > 25$ GeV we have obtained the following results for \mathcal{R} at NLO in QCD

$$\begin{aligned} \mathcal{R}(\mu_0 = m_t/2, \text{CT14}, p_{T,\gamma} > 25 \text{ GeV}) &= (4.56 \pm 0.25) \cdot 10^{-3} (5\%), \\ \mathcal{R}(\mu_0 = H_T/4, \text{CT14}, p_{T,\gamma} > 25 \text{ GeV}) &= (4.62 \pm 0.06) \cdot 10^{-3} (1\%), \end{aligned} \quad (5.3)$$

while for $p_{T,\gamma} > 50$ GeV our findings can be summarised as follows

$$\begin{aligned} \mathcal{R}(\mu_0 = m_t/2, \text{CT14}, p_{T,\gamma} > 50 \text{ GeV}) &= (1.89 \pm 0.16) \cdot 10^{-3} (8\%), \\ \mathcal{R}(\mu_0 = H_T/4, \text{CT14}, p_{T,\gamma} > 50 \text{ GeV}) &= (1.93 \pm 0.06) \cdot 10^{-3} (3\%). \end{aligned} \quad (5.4)$$

The observed change in the value of \mathcal{R} for the scale variation is truly asymmetric. Specifically, one of the estimated values is always below the quoted precision. Thus, similarly as

for absolute cross sections, theoretical errors, which are provided as well, are taken very conservatively as a maximum of these two results. Ratio results for our default $p_{T,\gamma}$ cut of 25 GeV for the two different scale choices are in perfect agreement within theoretical errors that are provided. This outcome is not affected by a higher value of the $p_{T,\gamma}$ cut, albeit, the absolute value of the ratio is smaller in the latter case. We notice that for $\mu_0 = m_t/2$ theoretical uncertainties from the scale variation are, indeed, below 10%, i.e. they are at the level of 5% and 8% respectively for the $p_{T,\gamma}$ cut of 25 GeV and 50 GeV. For $\mu_0 = H_T/4$, however, theoretical errors are substantially reduced down to 1% and 3%. Such precision is comparable to the precision one would rather expect from NNLO QCD results for top quark pair production. Thus, the ratio of $t\bar{t}\gamma$ and $t\bar{t}$ cross sections represents a very precise observable to be used at the LHC. One of the possible applications might be the measurement of the strength and the structure of the $t\bar{t}\gamma$ vertex in $t\bar{t}$ production. The latter could shed some light on possible new physics that can reveal itself only once sufficiently precise theoretical predictions are available.

Once again, if on-shell $t\bar{t}$ and $t\bar{t}\gamma$ production is employed to construct the cross section ratio

$$\mathcal{R}^{\text{on-shell}} = \frac{\sigma_{t\bar{t}\gamma}^{\text{NLO (on-shell)}}}{\sigma_{t\bar{t}}^{\text{NLO (on-shell)}}}, \quad (5.5)$$

no substantial reduction in the theoretical uncertainties could be observed when replacing $\mu_R = \mu_F = \mu_0 = m_t/2$ with $\mu_R = \mu_F = \mu_0 = E_T/4$. Indeed, we can write

$$\begin{aligned} \mathcal{R}^{\text{on-shell}}(\mu_0 = m_t/2, \text{CT14}, p_{T,\gamma} > 25 \text{ GeV}) &= (2.55 \pm 0.04) \cdot 10^{-3} (2\%), \\ \mathcal{R}^{\text{on-shell}}(\mu_0 = E_T/4, \text{CT14}, p_{T,\gamma} > 25 \text{ GeV}) &= (2.47 \pm 0.03) \cdot 10^{-3} (1\%). \end{aligned} \quad (5.6)$$

It is worth mentioning at this point that, the theoretical error for $\mathcal{R}^{\text{on-shell}}$ as calculated from the scale dependence is at the 2% level already for the fixed scale choice. From the experimental point of view, however, measurements in the phase space regions defined by the specific selection cuts that simulate as closely as possible detector response are more appropriate, simply because such measurements do not introduce additional and unnecessary uncertainties due to model-dependent extrapolations to parton level t and \bar{t} objects and to phase-space regions outside the detector sensitivity. Having on-shell results at hand we can also study the impact of top quark decays on the cross section ratio. We note that the central value of $\mathcal{R}^{\text{on-shell}}$ is smaller by a factor of 1.8 when comparing to \mathcal{R} . The cuts on the final state decay products in conjunction with hard photon emission from b -jets and charged leptons modify the ratio substantially. Since the set of selection cuts is different in both cases there is no particular reason why one would expect $\mathcal{R}^{\text{on-shell}}$ and \mathcal{R} to be equal.

To assess the PDF uncertainties, we have recalculated the \mathcal{R} observable for two different PDF sets, namely MMHT14 and NNPDF3.0 with $\mu_0 = m_t/2$. For $p_{T,\gamma} > 25$ GeV theoretical predictions for \mathcal{R} are given by

$$\begin{aligned} \mathcal{R}(\mu_0 = m_t/2, \text{MMHT14}, p_{T,\gamma} > 25 \text{ GeV}) &= (4.54 \pm 0.26) \cdot 10^{-3} (6\%), \\ \mathcal{R}(\mu_0 = m_t/2, \text{NNPDF3.0}, p_{T,\gamma} > 25 \text{ GeV}) &= (4.55 \pm 0.26) \cdot 10^{-3} (6\%), \end{aligned} \quad (5.7)$$

while for $p_{T,\gamma} > 50$ GeV we have found instead

$$\begin{aligned}\mathcal{R}(\mu_0 = m_t/2, \text{MMHT14}, p_{T,\gamma} > 50 \text{ GeV}) &= (1.87 \pm 0.17) \cdot 10^{-3} (9\%), \\ \mathcal{R}(\mu_0 = m_t/2, \text{NNPDF3.0}, p_{T,\gamma} > 50 \text{ GeV}) &= (1.88 \pm 0.17) \cdot 10^{-3} (9\%).\end{aligned}\tag{5.8}$$

We have estimated the size of the PDF uncertainties to be $\pm 0.02 \cdot 10^{-3}$ independently of the $p_{T,\gamma}$ cut. Thus, they are below 0.5% for $p_{T,\gamma} > 25$ GeV and of the order of 1% for $p_{T,\gamma} > 50$ GeV. For our best NLO QCD predictions for the \mathcal{R} observable with $\mu_0 = H_T/4$ theoretical uncertainties due to scale dependence are $\pm 0.06 \cdot 10^{-3}$, thus a factor of 3 larger than the PDF uncertainties. We have additionally computed internal PDF uncertainties for the cross section ratios. We have obtained $\pm 0.02 \cdot 10^{-3}$ for MMHT2014 and NNPDF3.0 as well as $\pm 0.04 \cdot 10^{-3}$ for CT14. In the latter case PDF uncertainties are of the order of 1% – 2% depending on the $p_{T,\gamma}$ cut, however, still a factor of 1.5 smaller than theoretical errors from the scale dependence for $\mu_0 = H_T/4$. Finally, our best NLO QCD predictions for the \mathcal{R} observable at the LHC with $\sqrt{s} = 13$ TeV are given by

$$\begin{aligned}\mathcal{R}(\mu_0 = H_T/4, \text{CT14}, p_{T,\gamma} > 25 \text{ GeV}) &= (4.62 \pm 0.06 [\text{scales}] \pm 0.04 [\text{PDFs}]) \cdot 10^{-3} \\ \mathcal{R}(\mu_0 = H_T/4, \text{CT14}, p_{T,\gamma} > 50 \text{ GeV}) &= (1.93 \pm 0.06 [\text{scales}] \pm 0.04 [\text{PDFs}]) \cdot 10^{-3},\end{aligned}\tag{5.9}$$

where we have included theoretical errors both from the scale dependence and from the PDFs. For the latter the internal PDF uncertainties as obtained for the default CT14 PDF set are quoted. Likewise for the \mathcal{R} observable the dominant source of theoretical systematics is associated with the scale dependence.

We would like to note here that a meaningful theoretical error on \mathcal{R} coming from the scale variation can be calculated for the first time only at NLO in QCD. At LO theoretical predictions for \mathcal{R} for the fixed scale choice and for the CT14 PDF set with $p_{T,\gamma} > 25$ GeV are given by

$$\mathcal{R}(\mu_0 = m_t/2, \text{CT14}, p_{T,\gamma} > 25 \text{ GeV}) = (4.94 \pm 0.08) \cdot 10^{-3} (2\%).\tag{5.10}$$

The scale variation of \mathcal{R} at LO is much smaller than at NLO. In the latter case we have obtained 5% instead. Since at LO we generate $pp \rightarrow t\bar{t}\gamma$ at $\mathcal{O}(\alpha_s^2\alpha^5)$ and $pp \rightarrow t\bar{t}$ at $\mathcal{O}(\alpha_s^2\alpha^4)$ we have the same order in α_s for both production processes and the dependence on $\alpha_s(\mu_R)$ cancels out in the cross section ratio. The only source of the scale dependence comes from variations in PDFs. The latter, however, also largely cancels out in the cross section ratio. The dependence on μ_R is introduced for the first time at NLO due to the virtual and the real corrections. Specifically, different one loop and real emission structures in both processes give us a handle on $\alpha_s(\mu_R)$. Additionally, the NLO predictions depend on the renormalisation scale through logarithms of μ_R , which appear in both the virtual and the real emission contributions. Thus, the LO error is truly underestimated and only the NLO theoretical error should be considered as reliable.

In the next step, we would like to study the effect of various settings in the numerator and denominator of the \mathcal{R} observable on the cross section ratio. In many experimental studies various MC programs are employed usually with the default scale choice implemented in

a given program. Thus, one should assess the size of the additional theoretical uncertainties due to the mismatch to see if they are substantial or can be simply ignored. To this end for the CT14 PDF set we calculate cross section ratios assuming different scale choices in the numerator (μ_1) and in the denominator (μ_2) of the \mathcal{R} observable. Specifically, we set μ_1 to the fixed scale choice $m_t/2$ and μ_2 to the dynamical scale choice $H_T/4$ and vice versa. With the $p_{T,\gamma} > 25$ GeV cut we have obtained the following results at NLO in QCD

$$\begin{aligned}\mathcal{R}\left(\frac{\mu_1 = m_t/2}{\mu_2 = H_T/4}, \text{CT14}, p_{T,\gamma} > 25 \text{ GeV}\right) &= (4.59 \pm 0.33) \cdot 10^{-3} (7\%), \\ \mathcal{R}\left(\frac{\mu_1 = H_T/4}{\mu_2 = m_t/2}, \text{CT14}, p_{T,\gamma} > 25 \text{ GeV}\right) &= (4.60 \pm 0.14) \cdot 10^{-3} (3\%).\end{aligned}\tag{5.11}$$

In the case of $p_{T,\gamma} > 50$ GeV cut our NLO QCD findings can be summarised as

$$\begin{aligned}\mathcal{R}\left(\frac{\mu_1 = m_t/2}{\mu_2 = H_T/4}, \text{CT14}, p_{T,\gamma} > 50 \text{ GeV}\right) &= (1.90 \pm 0.19) \cdot 10^{-3} (10\%), \\ \mathcal{R}\left(\frac{\mu_1 = H_T/4}{\mu_2 = m_t/2}, \text{CT14}, p_{T,\gamma} > 50 \text{ GeV}\right) &= (1.92 \pm 0.09) \cdot 10^{-3} (5\%).\end{aligned}\tag{5.12}$$

Even though in each case the central value of the cross section ratio has not been changed, we observe an increase of the theoretical error due to scale dependence. For the $p_{T,\gamma}$ cut of 25 GeV (50 GeV) the following increase of the relative error can be quoted: for $\mu_1 = m_t/2$ the rise from 5% (8%) to 7% (10%) and for $\mu_1 = H_T/4$ from 1% (3%) to 3% (5%). Therefore, in order to have $t\bar{t}\gamma$ production under excellent theoretical control the same scale choice should be employed for the generation of both processes $pp \rightarrow t\bar{t}\gamma$ and $pp \rightarrow t\bar{t}$. We can also study the impact of using various PDF sets for the \mathcal{R} observable. In that case our NLO QCD predictions for $p_{T,\gamma} > 25$ GeV are given by

$$\begin{aligned}\mathcal{R}\left(\mu_0 = m_t/2, \frac{\text{CT14}}{\text{MMHT14}}, p_{T,\gamma} > 25 \text{ GeV}\right) &= (4.50 \pm 0.23) \cdot 10^{-3} (5\%), \\ \mathcal{R}\left(\mu_0 = m_t/2, \frac{\text{MMHT14}}{\text{CT14}}, p_{T,\gamma} > 25 \text{ GeV}\right) &= (4.60 \pm 0.28) \cdot 10^{-3} (6\%). \\ \mathcal{R}\left(\mu_0 = m_t/2, \frac{\text{CT14}}{\text{NNPDF3.0}}, p_{T,\gamma} > 25 \text{ GeV}\right) &= (4.39 \pm 0.23) \cdot 10^{-3} (5\%), \\ \mathcal{R}\left(\mu_0 = m_t/2, \frac{\text{NNPDF3.0}}{\text{CT14}}, p_{T,\gamma} > 25 \text{ GeV}\right) &= (4.74 \pm 0.28) \cdot 10^{-3} (6\%).\end{aligned}\tag{5.13}$$

For $p_{T,\gamma} > 50$ GeV have obtained instead

$$\begin{aligned}
\mathcal{R}\left(\mu_0 = m_t/2, \frac{\text{CT14}}{\text{MMHT14}}, p_{T,\gamma} > 50 \text{ GeV}\right) &= (1.87 \pm 0.15) \cdot 10^{-3} (8\%), \\
\mathcal{R}\left(\mu_0 = m_t/2, \frac{\text{MMHT14}}{\text{CT14}}, p_{T,\gamma} > 50 \text{ GeV}\right) &= (1.90 \pm 0.17) \cdot 10^{-3} (9\%). \\
\mathcal{R}\left(\mu_0 = m_t/2, \frac{\text{CT14}}{\text{NNPDF3.0}}, p_{T,\gamma} > 50 \text{ GeV}\right) &= (1.82 \pm 0.15) \cdot 10^{-3} (8\%), \\
\mathcal{R}\left(\mu_0 = m_t/2, \frac{\text{NNPDF3.0}}{\text{CT14}}, p_{T,\gamma} > 50 \text{ GeV}\right) &= (1.96 \pm 0.18) \cdot 10^{-3} (9\%).
\end{aligned}
\tag{5.14}$$

Although the choice of various PDF sets in the cross section ratio is not theoretically very well motivated it does not affect the estimation of the theoretical errors. Overall, unlike the theoretical uncertainties due to the different scale choice, additional undesired PDF uncertainties are negligible. Let us note here, that the issue of choosing the same value of μ_0 for both production processes is going to play a crucial role when various differential cross section ratios will be constructed.

To summarise this part of the paper, we discuss the stability of the cross section ratio against higher order corrections. To this end we also comment on the size of NLO QCD corrections to the absolute $t\bar{t}$ and $t\bar{t}\gamma$ cross section with complete top quark off-shell effects included. With $\mu_R = \mu_F = \mu_0$ set to $\mu_0 = m_t/2$ and for the CT14 PDF set the full $pp \rightarrow t\bar{t}$ cross section receives negative and small NLO corrections of 3%. For $pp \rightarrow t\bar{t}\gamma$ we have obtained negative and moderate NLO corrections of 10% (13%) for the $p_{T,\gamma}$ cut of 25 GeV (50 GeV). The size of NLO QCD corrections to cross section ratio \mathcal{R} is similar to the $pp \rightarrow t\bar{t}\gamma$ case. Specifically, NLO QCD corrections are also negative and of the order of 8% and 11% depending on the $p_{T,\gamma}$ cut. For the dynamical scale choice $\mu_0 = H_T/2$ the NLO QCD corrections to $pp \rightarrow t\bar{t}$ are positive and very small of the order of 0.6% only. For the absolute $pp \rightarrow t\bar{t}\gamma$ cross section they are also positive and small, however, of the order of 2% and 5% for $p_{T,\gamma} > 25$ GeV and $p_{T,\gamma} > 50$ GeV respectively. The size of NLO QCD corrections to the \mathcal{R} observable as evaluated with $\mu_0 = H_T/4$ follows the same pattern as for the $t\bar{t}\gamma$ production process. Thus, the cross section ratio is very stable against higher order corrections and behaves similarly as the absolute $t\bar{t}\gamma$ cross section when NLO QCD corrections are incorporated.

6 Differential Cross Section Ratios at NLO in QCD

In the following we present results for differential cross section ratios defined according to

$$\mathcal{R}_X = \left(\frac{d\sigma_{t\bar{t}\gamma}^{\text{NLO}}(\mu_1)}{dX} \right) \left(\frac{d\sigma_{t\bar{t}}^{\text{NLO}}(\mu_2)}{dX} \right)^{-1},
\tag{6.1}$$

where X stands for the observable that is under scrutiny. In Figure 4 we present differential cross section distributions as a function of the invariant mass of two b -jets. Thus, in that

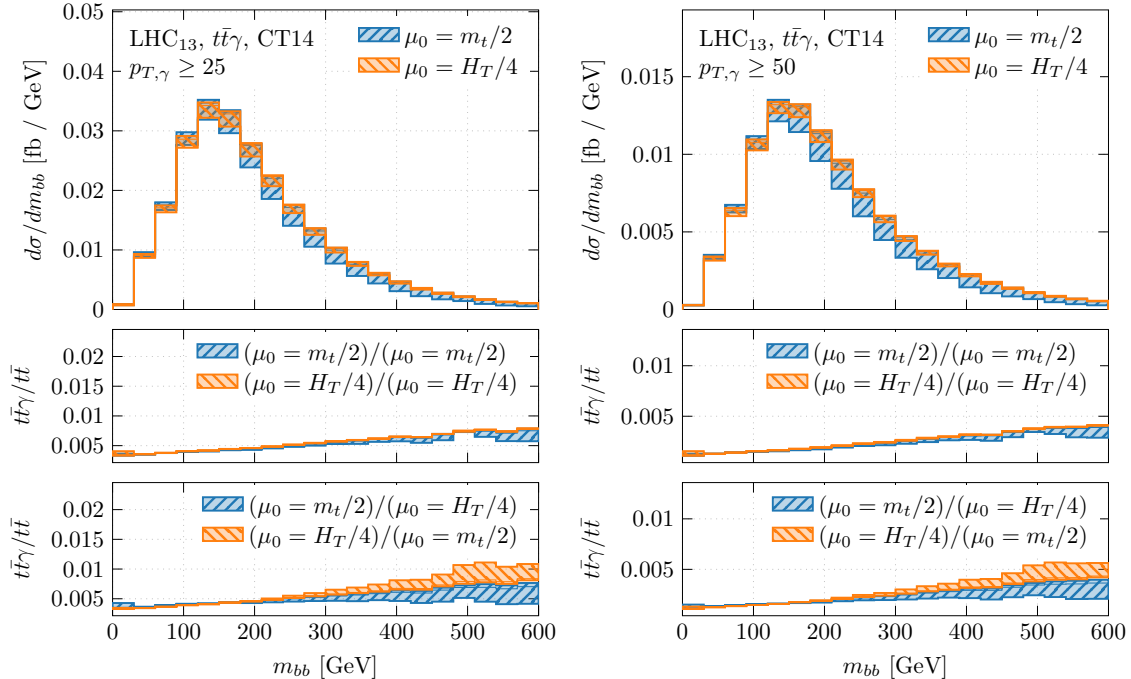


Figure 4. Differential cross section distributions as a function of the invariant mass of two b -jets for the $pp \rightarrow e^+ \nu_e \mu^- \bar{\nu}_\mu b \bar{b} \gamma + X$ process at the LHC run II with $\sqrt{s} = 13$ TeV. The upper plots show absolute NLO predictions for $p_{T,\gamma} > 25$ GeV (left panel) and $p_{T,\gamma} > 50$ GeV (right panel) together with the corresponding uncertainty bands resulting from scale variations. Renormalisation and factorisation scales are set to the common value $\mu_R = \mu_F = \mu_0$ where $\mu_0 = m_t/2$ and $H_T/4$. The CT14 PDF set is employed. The lower panels display differential cross section ratios together with their uncertainty bands. In the first case (middle panel), the same fixed (dynamical) scale choice is employed in the numerator and the denominator of the cross section ratio. In the second case (bottom panel), different scale choices in the numerator and in the denominator have been assumed.

case we have $X = m_{bb}$ and $\mathcal{R}_{m_{bb}}$. The upper plots show absolute NLO predictions for the $e^+ \nu_e \mu^- \bar{\nu}_\mu b \bar{b} \gamma + X$ production process at the LHC at the centre-of-mass energy of $\sqrt{s} = 13$ TeV. Results are given for $\mu_R = \mu_F = \mu_0$, where $\mu_0 = m_t/2$ or $\mu_0 = H_T/4$, for the CT14 PDF set and for two different values of the $p_{T,\gamma}$ cut, i.e. $p_{T,\gamma} > 25$ GeV and $p_{T,\gamma} > 50$ GeV. Also provided are corresponding uncertainty bands resulting from scale variations. The lower panels display differential cross section ratios together with their uncertainty bands. In the first case, that is presented in the middle panel, we have employed $\mu_1 = \mu_2 = \mu_0$, where $\mu_0 = m_t/2$ or $\mu_0 = H_T/4$. In the second case, which is shown in the bottom panel, $\mu_1 \neq \mu_2$ has been assumed. For that case two options are investigated, $(\mu_1 = m_t/2)/(\mu_2 = H_T/4)$ and $(\mu_1 = H_T/4)/(\mu_2 = m_t/2)$. For the fixed scale choice for both values of the $p_{T,\gamma}$ cut we have observed that the theoretical error due to scale dependence for the absolute differential cross section is in the range of 40% – 45% towards the end of the m_{bb} spectrum. On the other hand, for $\mu_0 = H_T/4$ theoretical uncertainties up to only 6% – 7% have been

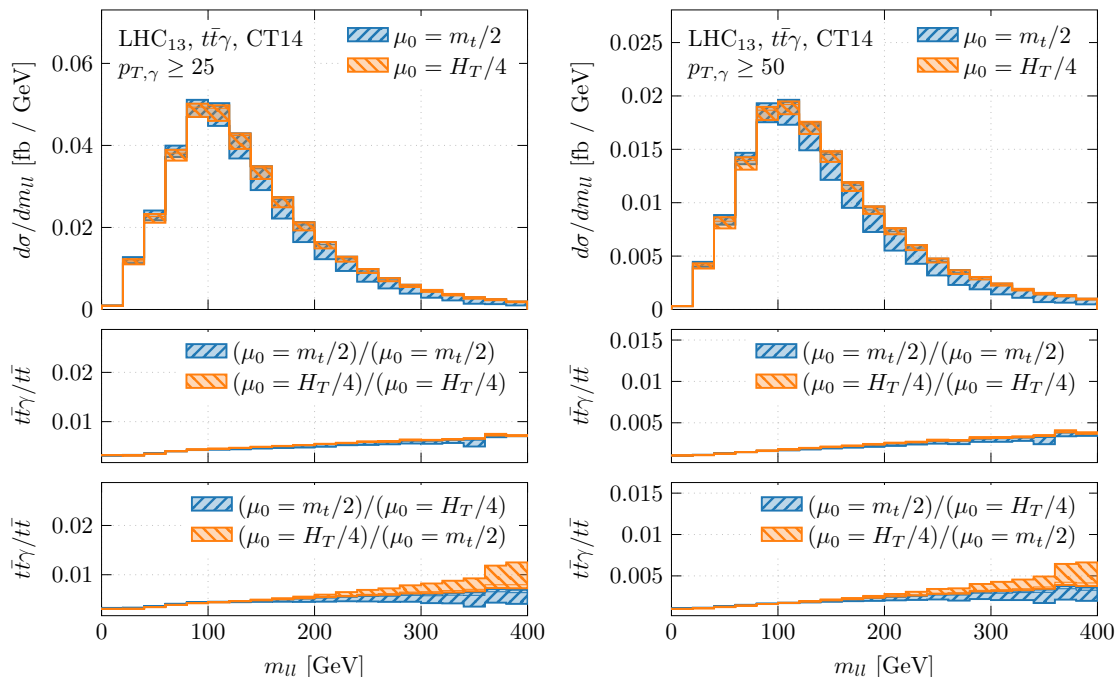


Figure 5. Differential cross section distributions as a function of the invariant mass of two charged leptons for the $pp \rightarrow e^+ \nu_e \mu^- \bar{\nu}_\mu b \bar{b} \gamma + X$ process at the LHC run II with $\sqrt{s} = 13$ TeV. The upper plots show absolute NLO predictions for $p_{T,\gamma} > 25$ GeV (left panel) and $p_{T,\gamma} > 50$ GeV (right panel) together with the corresponding uncertainty bands resulting from scale variations. Renormalisation and factorisation scales are set to the common value $\mu_R = \mu_F = \mu_0$ where $\mu_0 = m_t/2$ and $H_T/4$. The CT14 PDF set is employed. The lower panels display differential cross section ratios together with their uncertainty bands. In the first case (middle panel), the same fixed (dynamical) scale choice is employed in the numerator and the denominator of the cross section ratio. In the second case (bottom panel), different scale choices in the numerator and in the denominator have been assumed.

estimated in the same region. The situation is substantially changed when the cross section ratio, $\mathcal{R}_{m_{bb}}$, is studied instead. In the case of $\mu_1 = \mu_2 = \mu_0 = m_t/2$ a reduction almost by a factor of 2 can be noticed. Indeed, theoretical uncertainties of the order of 20% are estimated at the end of the m_{bb} spectrum. This finding is also independent of the $p_{T,\gamma}$ cut. For $\mu_1 = \mu_2 = \mu_0 = H_T/4$, however, one can acquire theoretical uncertainties of the order of 1% – 2% in the whole plotted range. This shows that the differential cross section ratio is also a very precise observable to be studied together with the total cross section ratio at the LHC to constrain physics beyond the SM for example via constraining anomalous top quark couplings. It can also be used to extract the electric charge of the top quark or the top quark charge asymmetry with a very high precision. When the scales μ_1 and μ_2 are chosen independently, however, the size of theoretical uncertainties has increased dramatically up to 30% – 40%, as can be clearly seen in Figure 4. Thus, choosing the same μ_0 in the numerator and denominator of $\mathcal{R}_{m_{bb}}$ is essential for building a high precision

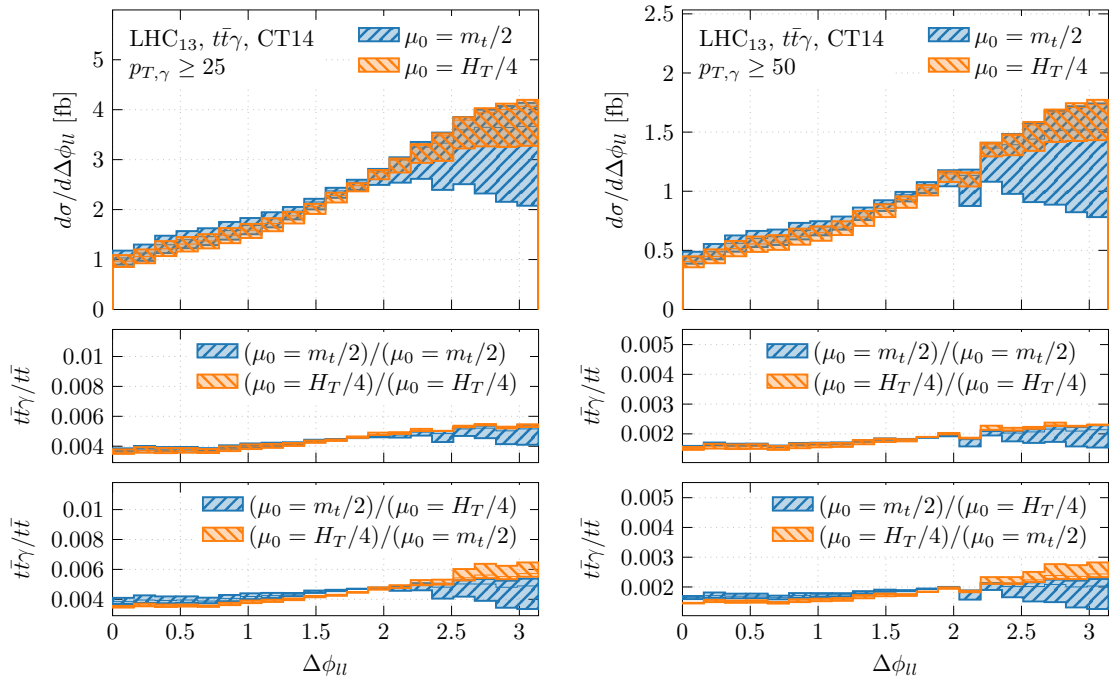


Figure 6. Differential cross section distributions as a function of $\Delta\phi_{\ell\ell}$ for the $pp \rightarrow e^+\nu_e\mu^-\bar{\nu}_\mu b\bar{b}\gamma + X$ process at the LHC run II with $\sqrt{s} = 13$ TeV. The upper plots show absolute NLO predictions for $p_{T,\gamma} > 25$ GeV (left panel) and $p_{T,\gamma} > 50$ GeV (right panel) together with the corresponding uncertainty bands resulting from scale variations. Renormalisation and factorisation scales are set to the common value $\mu_R = \mu_F = \mu_0$ where $\mu_0 = m_t/2$ and $H_T/4$. The CT14 PDF set is employed. The lower panels display differential cross section ratios together with their uncertainty bands. In the first case (middle panel), the same fixed (dynamical) scale choice is employed in the numerator and the denominator of the cross section ratio. In the second case (bottom panel), different scale choices in the numerator and in the denominator have been assumed.

observable, otherwise the theoretical errors are drastically overestimated.

Similar conclusions can be drawn for the differential cross section distribution as a function of the invariant mass of two charged leptons. This observable is plotted in Figure 5 again for $p_{T,\gamma} > 25$ GeV and $p_{T,\gamma} > 50$ GeV. The advantage of this observable in comparison to the invariant mass of two b -jets lies, however, in the fact that measurements of lepton kinematic observables are particularly precise at the LHC due to the excellent lepton energy resolution of the ATLAS and CMS detectors. Moreover, the reconstruction of the top quarks is not required to construct $m_{\ell\ell}$. For m_{bb} , on the other hand, good b -jet tagging efficiency and low light jet misstag rate is mandatory. For the cross section ratio, $\mathcal{R}_{m_{\ell\ell}}$, with the dynamical scale choice $\mu_1 = \mu_2 = H_T/4$ (the fixed scale choice $\mu_1 = \mu_2 = m_t/2$) the theoretical uncertainties of the order of 1% – 4% (20% – 25%) have been estimated. These should be compared to uncertainties of up to 10% (50%) for the absolute differential cross section. Again, our findings mildly depend on the $p_{T,\gamma}$ cut. When different scales are applied to the numerator and the denominator of $\mathcal{R}_{m_{\ell\ell}}$ theoretical uncertainties in the tail

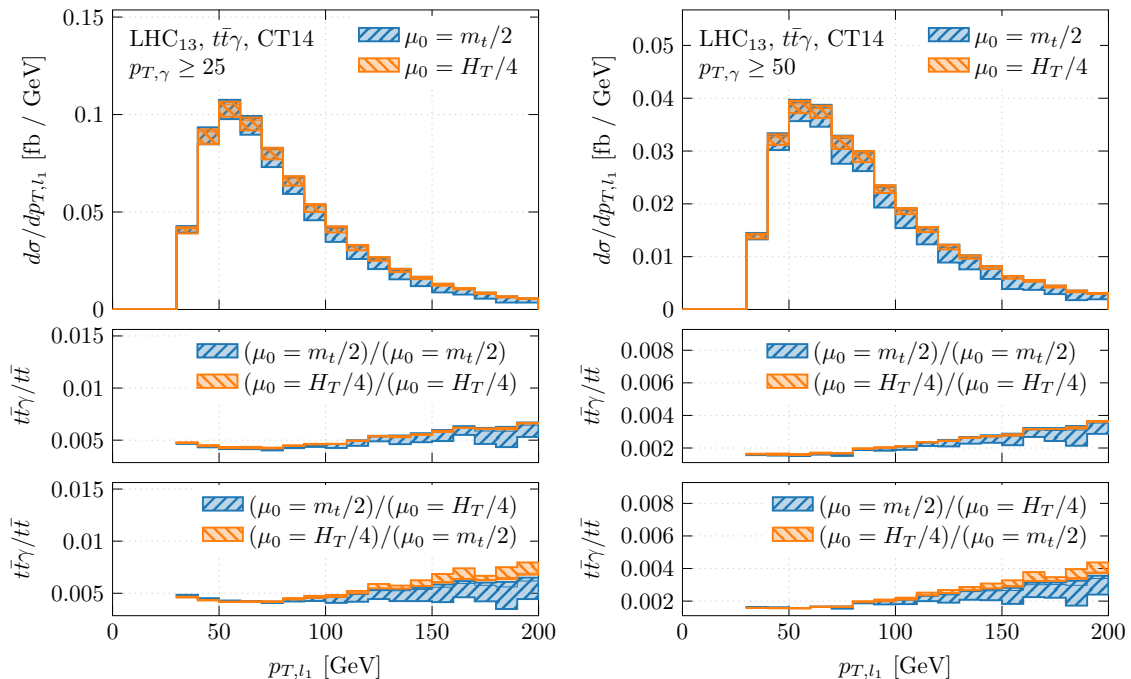


Figure 7. Differential cross section distributions as a function of the transverse momentum of the hardest charged lepton for the $pp \rightarrow e^+ \nu_e \mu^- \bar{\nu}_\mu b \bar{b} \gamma + X$ process at the LHC run II with $\sqrt{s} = 13$ TeV. The upper plots show absolute NLO predictions for $p_{T,\gamma} > 25$ GeV (left panel) and $p_{T,\gamma} > 50$ GeV (right panel) together with the corresponding uncertainty bands resulting from scale variations. Renormalisation and factorisation scales are set to the common value $\mu_R = \mu_F = \mu_0$ where $\mu_0 = m_t/2$ and $H_T/4$. The CT14 PDF sets are employed. The lower panels display differential cross section ratios together with their uncertainty bands. In the first case (middle panel), the same fixed (dynamical) scale choice is employed in the numerator and the denominator of the cross section ratio. In the second case (bottom panel), different scale choices in the numerator and in the denominator have been assumed.

of the distribution have increased up to 35% – 40% for $\mu_1 = m_t/2$ and $\mu_2 = H_T/4$ whereas in the case of $\mu_1 = H_T/4$ and $\mu_2 = m_t/2$ they are in the range of 50% – 60%.

In Figure 6 the differential cross section distribution as a function of the difference in azimuthal angle between the two charged leptons, $\Delta\phi_{\ell\ell} = |\phi_{\ell_1} - \phi_{\ell_2}|$, is presented. The $\Delta\phi_{\ell\ell}$ observable is also measured very precisely at the LHC by both the ATLAS and CMS collaborations. It can be used for example to construct the leptonic charge asymmetry, $A_C^{\ell\ell}$, which is sensitive to signals of numerous beyond the SM scenarios, where among others new heavy states might be produced. In general, angular distributions of charged leptons are of huge importance since they reflect spin correlations of the top quark pair and can be employed to probe the CP numbers of such new states, see e.g. [36–40]. For the fixed (dynamical) scale choice theoretical uncertainties for $\Delta\phi_{\ell\ell}$ in the region given by $\Delta\phi_{\ell\ell} \gtrsim 2.5$ are of the order of 40% – 50% (15% – 20%) depending on the transverse momentum cut on the hard photon. When the cross section ratio $\mathcal{R}_{\Delta\phi_{\ell\ell}}$ is investigated

instead theoretical errors of 20% – 30% for $\mu_0 = m_t/2$ and 2% – 3% for $\mu_0 = H_T/4$ can be estimated in that region. Overall, for $\Delta\phi_{\ell\ell} \in (0, \pi)$ with $\mu_0 = m_t/2$ or with $\mu_0 = H_T/4$ theoretical uncertainties for $\mathcal{R}_{\Delta\phi_{\ell\ell}}$ are in the range 1% – 30%, 1% – 6% respectively. As in the previous cases when $\mu_1 \neq \mu_2$ is set instead substantial overestimation of the theoretical uncertainties can be observed for $\mathcal{R}_{\Delta\phi_{\ell\ell}}$. For example for $\Delta\phi_{\ell\ell} \gtrsim 2.5$ an increase from 20% – 30% up to 30% – 40% has been procured once $\mu_1 = m_t/2$ and $\mu_2 = H_T/4$ have been assumed, while for $\mu_1 = H_T/4$ and $\mu_2 = m_t/2$ we have obtained a change from 2% – 3% to 15%.

Finally, in Figure 7 the differential cross section as a function of the transverse momentum of the hardest charged lepton is shown. This observable is also sensitive to effects of possible new physics beyond the SM, see e.g. [41]. Among others, it can be used to test exotic physics scenarios where top like quarks with the electric charge of $Q_t = -4/3$ might be produced. For the absolute $t\bar{t}\gamma$ cross section theoretical uncertainties are up to 30% – 45% for $\mu_0 = m_t/2$ and up to 8% for $\mu_0 = H_T/4$. Once the cross section ratio, $\mathcal{R}_{p_{T,\ell_1}}$, is investigated theoretical uncertainties have been substantially reduced down to 20% – 30% for the fixed scale choice and to 4% – 5% for the phase-space dependent scale choice. If we assume different scales in $\mathcal{R}_{p_{T,\ell_1}}$, i.e. $\mu_1 = m_t/2$ and $\mu_2 = H_T/4$, theoretical errors comparable to these quoted for the absolute $t\bar{t}\gamma$ cross sections with $\mu_0 = m_t/2$ have been evaluated. On the other hand, setting $\mu_1 = H_T/4$ and $\mu_2 = m_t/2$, has resulted in theoretical uncertainties for $\mathcal{R}_{p_{T,\ell_1}}$ maximally up to 15%.

To summarise this part of the paper, the theoretical uncertainties due to scale dependence of the order of 1% – 6% have been obtained for the studied cross section ratios if $\mu_1 = \mu_2 = \mu_0 = H_T/4$ has been employed to construct \mathcal{R}_X , where X stands for $X = m_{b\bar{b}}, m_{\ell\ell}, \Delta\phi_{\ell\ell}, p_{T,\ell_1}$. Let us mention at this point that also for differential cross section ratios the PDF uncertainties are smaller than the theoretical uncertainties due to scale dependence. The latter remains the dominant source of theoretical uncertainties.

7 Conclusions

The purpose of the paper is to obtain more precise theoretical predictions for $t\bar{t}\gamma$ production in the di-lepton top quark decay channel for the LHC Run II energy of $\sqrt{s} = 13$ TeV without the need of including terms beyond NLO in the perturbation expansion in α_s . To this end cross section ratios $\mathcal{R} = \sigma_{pp \rightarrow t\bar{t}\gamma}^{\text{NLO}}(\mu_1)/\sigma_{pp \rightarrow t\bar{t}}^{\text{NLO}}(\mu_2)$ have been studied. Fully realistic NLO computations for $t\bar{t}$ and $t\bar{t}\gamma$ production have been employed. They are based on LO and NLO matrix elements for $e^+\nu_e\mu^-\bar{\nu}_\mu b\bar{b}$ and $e^+\nu_e\mu^-\bar{\nu}_\mu b\bar{b}\gamma$ production processes that include all resonant and non-resonant top quark and W gauge boson Feynman diagrams, interferences, and off-shell effects of t and W . Various renormalisation and factorisation scale choices and parton density functions have been examined to assess their impact on the cross section ratio. Our best NLO QCD predictions for the \mathcal{R} observable have been obtained for $\mu_1 = \mu_2 = \mu_0 = H_T/4$ and can be summarised as follows

$$\begin{aligned} \mathcal{R}(\mu_0 = H_T/4, \text{CT14}, p_{T,\gamma} > 25 \text{ GeV}) &= (4.62 \pm 0.06 [\text{scales}] \pm 0.04 [\text{PDFs}]) \cdot 10^{-3} \\ \mathcal{R}(\mu_0 = H_T/4, \text{CT14}, p_{T,\gamma} > 50 \text{ GeV}) &= (1.93 \pm 0.06 [\text{scales}] \pm 0.04 [\text{PDFs}]) \cdot 10^{-3}. \end{aligned} \quad (7.1)$$

The theoretical uncertainties due to scale dependence have been estimated to be above 1% for $p_{T,\gamma} > 25$ GeV and of the order of 3% for $p_{T,\gamma} > 50$ GeV. The theoretical uncertainties due to various PDF parameterisations, on the other hand, are 0.5% and 1% respectively. When the internal PDF uncertainties are extracted from the CT14 PDF set following the prescription of the CT14 PDF collaboration then they are slightly higher, namely below 1% and of the order of 2% for $p_{T,\gamma} > 25$ GeV and $p_{T,\gamma} > 50$ GeV respectively. The latter are quoted for our best theoretical predictions. Nevertheless, they are still smaller than theoretical errors from the scale dependence. Regardless of which uncertainty we will assign for PDF uncertainties such small theoretical uncertainties are normally available only in the case of top quark pair production at NNLO in QCD. Thus, the cross section ratio has proven to be a very precise observable that should be measured at the LHC. There are many possible applications, including, but not limited to, precise measurements of the top quark charge as well as searches for new physics effects that can reveal themselves only when a few percent precision on the theory side is available. For the fixed scale choice, which is still commonly used in experimental analyses, our finding for $\mu_1 = \mu_2 = \mu_0 = m_t/2$ are given by

$$\begin{aligned}\mathcal{R}(\mu_0 = m_t/2, \text{CT14}, p_{T,\gamma} > 25 \text{ GeV}) &= (4.56 \pm 0.25 [\text{scales}] \pm 0.04 [\text{PDFs}]) \cdot 10^{-3}, \\ \mathcal{R}(\mu_0 = m_t/2, \text{CT14}, p_{T,\gamma} > 50 \text{ GeV}) &= (1.89 \pm 0.16 [\text{scales}] \pm 0.04 [\text{PDFs}]) \cdot 10^{-3}.\end{aligned}\tag{7.2}$$

Also in this case theoretical errors due to scale dependence of the order of a few percent, 5% for $p_{T,\gamma} > 25$ GeV and 8% for $p_{T,\gamma} > 50$ GeV, have been estimated. We have also shown that such high precision can only be obtained if μ_1 and μ_2 are set to a common scale. Otherwise, theoretical uncertainties from the scale dependence are overestimated. We have argued on the similarity of the two processes, that using the same scale for both is well justified.

Subsequently, we have turned our attention to differential cross section distributions. Four observables have been presented at the differential level for the $t\bar{t}\gamma$ production process at the LHC. Specifically, we have shown the invariant mass of two b -jets (m_{bb}), the invariant mass of two charged leptons ($m_{\ell\ell}$), the difference in azimuthal angle between two charged leptons ($\Delta\phi_{\ell\ell}$) and the transverse momentum of the hardest charged lepton (p_{T,ℓ_1}). Afterwards, we have calculated differential cross section ratios for these observables according to

$$\mathcal{R}_X = \left(\frac{d\sigma_{t\bar{t}\gamma}^{\text{NLO}}(\mu_1)}{dX} \right) \left(\frac{d\sigma_{t\bar{t}}^{\text{NLO}}(\mu_2)}{dX} \right)^{-1},\tag{7.3}$$

where $X = m_{bb}, m_{\ell\ell}, \Delta\phi_{\ell\ell}$ and p_{T,ℓ_1} . A clear conclusion could be drawn from our considerations. For observables that we have presented, which are also important for beyond the SM physics searches, the most precise predictions for \mathcal{R}_X have been obtained for $\mu_1 = \mu_2 = \mu_0$. Especially interesting conclusions have been reached for the case of the dynamical scale choice, i.e. $\mu_0 = H_T/4$. For all observables that have been investigated, theoretical uncertainties due to scale dependence, which are the dominant source of theoretical systematics also at the differential level, are in the 1%–6% range. These findings are independent of the

transverse momentum cut on the isolated hard photon. Such precise theoretical predictions at the differential level should be now employed to indirectly search for new physics at the LHC. When different scale choices $\mu_1 \neq \mu_2$ for \mathcal{R}_X have been assumed instead, theoretical uncertainties have been dramatically overestimated. Thus, care must be taken to ensure that μ_1 and μ_2 are as similar as possible when building the \mathcal{R}_X observables to be used in experimental studies. Based on our studies we advocate for the H_T based scale choice for μ_1 and μ_2 in \mathcal{R}_X . Definitely, mixing dynamical and fixed scales in $t\bar{t}\gamma$ and $t\bar{t}$ production introduces additional and unnecessary theoretical uncertainties that should be avoided.

As a further matter let us note here that, from the experimental point of view measurements in the fiducial phase space, which is the phase space defined by the specific selection cuts that simulate detector response as closely as possible, are the most appropriate for new physics searches in the top quark sector and for precision measurements of top quark properties within the SM theory of particle physics. The reason being that such measurements do not introduce additional and unnecessary systematic uncertainties due to model-dependent extrapolations to parton level t and \bar{t} objects and to phase-space regions outside the detector sensitivity. Therefore, our theoretical predictions for observables like $\mathcal{R}_{m_{\ell\ell}}$, $\mathcal{R}_{\Delta\phi_{\ell\ell}}$ and $\mathcal{R}_{p_{T,\ell_1}}$ might be directly compared with experimental data at the fiducial level that are collected at the LHC by the ATLAS and CMS experimental collaborations. These leptonic observables should be marginally affected by parton shower effects. Firstly, such effects are milder if the underlying computations are NLO accurate since the fixed order contribution already includes part of the radiation simulated by the shower. Secondly, leptonic observables are rather stable against shower effects, see e.g. Ref. [42], as compared for example to observables, which are build out of light- and b -jets. Nevertheless, due to the fact that both processes are very similar from the QCD point of view such effects should cancel to a large extent in cross section ratios. Regardless, let us mention at this point that recently a new method for matching NLO QCD calculations to parton shower programs has been proposed [43], which incorporates top quark finite width effects in the shower approach together with all interference effects. Specifically, it allows for a consistent treatment of resonances in the POWHEG framework by preserving the mass of top-quark resonances near their peak. First results for the simplest case of the $e^+\nu_e\mu^-\bar{\nu}b\bar{b}$ production process have been already presented in Ref. [44]. Until now, however, this method has not been applied to the more complex process $e^+\nu_e\mu^-\bar{\nu}b\bar{b}\gamma$. Once available it can be used for studying $\sigma_{e^+\nu_e\mu^-\bar{\nu}b\bar{b}\gamma}/\sigma_{e^+\nu_e\mu^-\bar{\nu}b\bar{b}}$.

Finally, let us also add that we have not investigated the impact of NLO electroweak corrections on $\sigma_{e^+\nu_e\mu^-\bar{\nu}b\bar{b}\gamma}/\sigma_{e^+\nu_e\mu^-\bar{\nu}b\bar{b}}$. However, based on results for the simpler $e^+\nu_e\mu^-\bar{\nu}b\bar{b}$ production process at the LHC with $\sqrt{s} = 13$ TeV [45], the ratio observable is not expected to be very sensitive to such effects. For the integrated cross section, NLO electroweak corrections to off-shell top anti-top production with leptonic decays are below 1%. In the case of differential cross sections such effects are small as well. Specifically, for $\Delta\phi_{\ell\ell}$ and $p_{T,\ell}$, which are studied in Ref. [45], NLO electroweak corrections are respectively below 1% and 2% (in the plotted range, i.e. up to 200 GeV for $p_{T,\ell}$). For the latter case they increase up to 7% when $p_{T,\ell} \approx 800$ GeV. Nevertheless, their size is substantially smaller than the size of NLO QCD corrections in the same regions. Furthermore, we expect that NLO electroweak

effects will be additionally minimised once \mathcal{R} and \mathcal{R}_X ratios are constructed. For the more complicated process $e^+\nu_e\mu^-\bar{\nu}b\bar{b}\gamma$ NLO electroweak calculations are not available in the literature. Up to now only NLO electroweak corrections to the on-shell $t\bar{t}\gamma$ production process have been evaluated [46]. Nevertheless, for the integrated $t\bar{t}\gamma$ cross section at the LHC with $\sqrt{s} = 13$ TeV and for the $p_{T,\ell} > 50$ GeV cut these corrections are below 2%. For various differential distributions presented in Ref. [46], like for example $p_{T,t}$ and $p_{T,\gamma}$, these effects are well below 10% even in the tails of these distributions. Based on that and the fact that further reduction is foreseen once \mathcal{R} and \mathcal{R}_X are built up out of the integrated and differential cross sections for the $e^+\nu_e\mu^-\bar{\nu}b\bar{b}\gamma$ and $e^+\nu_e\mu^-\bar{\nu}b\bar{b}$ production processes, we expect that our results for \mathcal{R} and \mathcal{R}_X will not be changed substantially.

On the technical side let us mention that all our results have been generated with the help of the HELAC-NLO MC framework. The final results are available (upon request) as Ntuple files [47]. In detail, they are stored in the form of modified Les Houches [48] and ROOT event files [49] that might be directly used for experimental studies at the LHC.

Acknowledgements

The work of M.W. and T.W. was supported in part by the DFG Research Grant "*Top-Quarks under the LHCs Magnifying Glass: From Process Modelling to Parameter Extraction*".

The work of H.B.H. has received funding from the European Research Council (ERC) under the European Union's Horizon 2020 research and innovation programme (grant agreement No 772099). Additionally, he has been supported by Rutherford Grant ST/M004104/1.

The research of G.B. was supported by grant K 125105 of the National Research, Development and Innovation Office in Hungary.

Simulations were performed with computing resources that are granted by RWTH Aachen University under project `rwth0211`.

References

- [1] G. Aad *et al.* [ATLAS Collaboration], *Observation of top-quark pair production in association with a photon and measurement of the $t\bar{t}\gamma$ production cross section in pp collisions at $\sqrt{s} = 7$ TeV using the ATLAS detector*, Phys. Rev. D **91** (2015) no.7, 072007 [[arXiv:1502.00586](#) [[hep-ex](#)]].
- [2] A. M. Sirunyan *et al.* [CMS Collaboration], *Measurement of the semileptonic $t\bar{t} + \gamma$ production cross section in pp collisions at $\sqrt{s} = 8$ TeV*, JHEP **1710** (2017) 006 [[arXiv:1706.08128](#) [[hep-ex](#)]].
- [3] M. Aaboud *et al.* [ATLAS Collaboration], *Measurement of the $t\bar{t}\gamma$ production cross section in proton-proton collisions at $\sqrt{s} = 8$ TeV with the ATLAS detector*, JHEP **1711** (2017) 086 [[1706.03046](#) [[hep-ex](#)]].
- [4] O. Bessidskaia Bylund, F. Maltoni, I. Tsirikos, E. Vryonidou and C. Zhang, *Probing top quark neutral couplings in the Standard Model Effective Field Theory at NLO in QCD*, JHEP **1605** (2016) 052 [[arXiv:1601.08193](#) [[hep-ph](#)]].

- [5] M. Schulze and Y. Soreq, *Pinning down electroweak dipole operators of the top quark*, Eur. Phys. J. C **76** (2016) no.8, 466 [[arXiv:1603.08911](#) [[hep-ph](#)]].
- [6] G. Bevilacqua, H. B. Hartanto, M. Kraus, T. Weber and M. Worek, *Hard Photons in Hadroproduction of Top Quarks with Realistic Final States*, JHEP **1810** (2018) 158 [[arXiv:1803.09916](#) [[hep-ph](#)]].
- [7] A. Denner, S. Dittmaier, S. Kallweit and S. Pozzorini, *NLO QCD corrections to WWbb production at hadron colliders* Phys. Rev. Lett. **106** (2011) 052001 [[arXiv:1012.3975](#) [[hep-ph](#)]].
- [8] G. Bevilacqua, M. Czakon, A. van Hameren, C. G. Papadopoulos and M. Worek, *Complete off-shell effects in top quark pair hadroproduction with leptonic decay at next-to-leading order* JHEP **1102** (2011) 083 [[arXiv:1012.4230](#) [[hep-ph](#)]].
- [9] A. Denner, S. Dittmaier, S. Kallweit and S. Pozzorini, *NLO QCD corrections to off-shell top-antitop production with leptonic decays at hadron colliders* JHEP **1210** (2012) 110 [[arXiv:1207.5018](#) [[hep-ph](#)]].
- [10] G. Bevilacqua, M. Czakon, M. V. Garzelli, A. van Hameren, A. Kardos, C. G. Papadopoulos, R. Pittau and M. Worek, *Helac-NLO*, Comput. Phys. Commun. **184** (2013) 986 [[arXiv:1110.1499](#) [[hep-ph](#)]].
- [11] A. van Hameren, C. G. Papadopoulos and R. Pittau, *Automated one-loop calculations: A Proof of concept*, JHEP **0909** (2009) 106 [[arXiv:0903.4665](#) [[hep-ph](#)]].
- [12] G. Ossola, C. G. Papadopoulos and R. Pittau, *CutTools: A Program implementing the OPP reduction method to compute one-loop amplitudes*, JHEP **0803** (2008) 042 [[arXiv:0711.3596](#) [[hep-ph](#)]].
- [13] M. Czakon, C. G. Papadopoulos and M. Worek, *Polarizing the Dipoles*, JHEP **0908** (2009) 085 [[arXiv:0905.0883](#) [[hep-ph](#)]].
- [14] G. Bevilacqua, M. Czakon, M. Kubocz and M. Worek, *Complete Nagy-Soper subtraction for next-to-leading order calculations in QCD*, JHEP **1310** (2013) 204 [[arXiv:1308.5605](#) [[hep-ph](#)]].
- [15] S. Catani and M. H. Seymour, *A General algorithm for calculating jet cross-sections in NLO QCD*, Nucl. Phys. B **485** (1997) 291, Erratum: [Nucl. Phys. B **510** (1998) 503] [[hep-ph/9605323](#)].
- [16] S. Catani, S. Dittmaier, M. H. Seymour and Z. Trocsanyi, *The Dipole formalism for next-to-leading order QCD calculations with massive partons*, Nucl. Phys. B **627** (2002) 189 [[hep-ph/0201036](#)].
- [17] A. van Hameren, *Kaleu: A General-Purpose Parton-Level Phase Space Generator*, [[arXiv:1003.4953](#) [[hep-ph](#)]].
- [18] A. Denner, S. Dittmaier, M. Roth and D. Wackerth, *Predictions for all processes $e^+e^- \rightarrow 4 \text{ fermions} + \gamma$* , Nucl. Phys. B **560** (1999) 33 [[hep-ph/9904472](#)].
- [19] A. Denner, S. Dittmaier, M. Roth and L. H. Wieders, *Electroweak corrections to charged-current $e^+e^- \rightarrow 4 \text{ fermion}$ processes: Technical details and further results*, Nucl. Phys. B **724** (2005) 247, Erratum: [Nucl. Phys. B **854** (2012) 504] [[hep-ph/0505042](#)].
- [20] A. van Hameren, *OneLoop: For the evaluation of one-loop scalar functions*, Comput. Phys. Commun. **182** (2011) 2427 [[arXiv:1007.4716](#) [[hep-ph](#)]].

- [21] G. Bevilacqua, H. B. Hartanto, M. Kraus and M. Worek, *Top Quark Pair Production in Association with a Jet with Next-to-Leading-Order QCD Off-Shell Effects at the Large Hadron Collider*, Phys. Rev. Lett. **116** (2016) no.5, 052003 [[arXiv:1509.09242](#) [[hep-ph](#)]].
- [22] G. Bevilacqua, H. B. Hartanto, M. Kraus and M. Worek, *Off-shell Top Quarks with One Jet at the LHC: A comprehensive analysis at NLO QCD*, JHEP **1611** (2016) 098 [[arXiv:1609.01659](#) [[hep-ph](#)]].
- [23] A. Buckley, J. Ferrando, S. Lloyd, K. Nordström, B. Page, M. Rüfenacht, M. Schönherr and G. Watt, *LHAPDF6: parton density access in the LHC precision era*, Eur. Phys. J. C **75** (2015) 132 [[arXiv:1412.7420](#) [[hep-ph](#)]].
- [24] J. Butterworth *et al.*, *PDF4LHC recommendations for LHC Run II*, J. Phys. G **43** (2016) 023001 [[arXiv:1510.03865](#) [[hep-ph](#)]].
- [25] S. Dulat *et al.*, *New parton distribution functions from a global analysis of quantum chromodynamics*, Phys. Rev. D **93** (2016) no.3, 033006 [[arXiv:1506.07443](#) [[hep-ph](#)]].
- [26] L. A. Harland-Lang, A. D. Martin, P. Motylinski and R. S. Thorne, *Parton distributions in the LHC era: MMHT 2014 PDFs*, Eur. Phys. J. C **75** (2015) no.5, 204 [[arXiv:1412.3989](#) [[hep-ph](#)]].
- [27] R. D. Ball *et al.* [NNPDF Collaboration], *Parton distributions for the LHC Run II*, JHEP **1504** (2015) 040 [[arXiv:1410.8849](#) [[hep-ph](#)]].
- [28] M. Cacciari, G. P. Salam and G. Soyez, *The Anti- $k(t)$ jet clustering algorithm*, JHEP **0804** (2008) 063 [[arXiv:0802.1189](#) [[hep-ph](#)]].
- [29] S. Frixione, *Isolated photons in perturbative QCD*, Phys. Lett. B **429** (1998) 369 [[hep-ph/9801442](#)].
- [30] R. Bonciani, S. Catani, M. L. Mangano and P. Nason, *NLL resummation of the heavy quark hadroproduction cross-section*, Nucl. Phys. B **529** (1998) 424 Erratum: [Nucl. Phys. B **803** (2008) 234] [[hep-ph/9801375](#)].
- [31] M. Czakon, D. Heymes and A. Mitov, *Dynamical scales for multi-TeV top-pair production at the LHC*, JHEP **1704** (2017) 071 [[arXiv:1606.03350](#) [[hep-ph](#)]].
- [32] M. Czakon and A. Mitov, *Top $^{++}$: A Program for the Calculation of the Top-Pair Cross-Section at Hadron Colliders*, Comput. Phys. Commun. **185** (2014) 2930 [[arXiv:1112.5675](#) [[hep-ph](#)]].
- [33] P. Bärnreuther, M. Czakon and A. Mitov, *Percent Level Precision Physics at the Tevatron: First Genuine NNLO QCD Corrections to $q\bar{q} \rightarrow t\bar{t} + X$* , Phys. Rev. Lett. **109** (2012) 132001 [[arXiv:1204.5201](#) [[hep-ph](#)]].
- [34] M. Czakon, P. Fiedler and A. Mitov, *Total Top-Quark Pair-Production Cross Section at Hadron Colliders Through $\mathcal{O}(\alpha_s^4)$* , Phys. Rev. Lett. **110** (2013) 252004 [[arXiv:1303.6254](#) [[hep-ph](#)]].
- [35] G. Bevilacqua and M. Worek, *On the ratio of $t\bar{t}b\bar{b}$ and $t\bar{t}jj$ cross sections at the CERN Large Hadron Collider*, JHEP **1407** (2014) 135 [[arXiv:1403.2046](#) [[hep-ph](#)]].
- [36] R. Frederix and F. Maltoni, *Top pair invariant mass distribution: A Window on new physics*, JHEP **0901** (2009) 047 [[arXiv:0712.2355](#) [[hep-ph](#)]].

- [37] W. Bernreuther and Z. G. Si, *Distributions and correlations for top quark pair production and decay at the Tevatron and LHC*, Nucl. Phys. B **837** (2010) 90 [[arXiv:1003.3926](#) [[hep-ph](#)]].
- [38] W. Bernreuther and Z. G. Si, *Top quark spin correlations and polarization at the LHC: standard model predictions and effects of anomalous top chromo moments*, Phys. Lett. B **725** (2013) 115 Erratum: [Phys. Lett. B **744** (2015) 413] [[arXiv:1305.2066](#) [[hep-ph](#)]].
- [39] G. Cacciapaglia, H. Cai, A. Deandrea, T. Flacke, S. J. Lee and A. Parolini, *Composite scalars at the LHC: the Higgs, the Sextet and the Octet*, JHEP **1511** (2015) 201 [[arXiv:1507.02283](#) [[hep-ph](#)]].
- [40] R. M. Godbole, G. Mendiratta and S. Rindani, *Looking for bSM physics using top-quark polarization and decay-lepton kinematic asymmetries*, Phys. Rev. D **92** (2015) no.9, 094013 [[arXiv:1506.07486](#) [[hep-ph](#)]].
- [41] K. Melnikov, M. Schulze and A. Scharf, *QCD corrections to top quark pair production in association with a photon at hadron colliders*, Phys. Rev. D **83** (2011) 074013 [[arXiv:1102.1967](#) [[hep-ph](#)]].
- [42] G. Heinrich, A. Maier, R. Nisius, J. Schlenk, M. Schulze, L. Scyboz and J. Winter, *NLO and off-shell effects in top quark mass determinations*, JHEP **1807** (2018) 129 [[arXiv:1709.08615](#) [[hep-ph](#)]].
- [43] T. Jezo and P. Nason, *On the Treatment of Resonances in Next-to-Leading Order Calculations Matched to a Parton Shower*, JHEP **1512** (2015) 065 [[arXiv:1509.09071](#) [[hep-ph](#)]].
- [44] T. Jezo, J. M. Lindert, P. Nason, C. Oleari and S. Pozzorini, *An NLO+PS generator for $t\bar{t}$ and Wt production and decay including non-resonant and interference effects*, Eur. Phys. J. C **76** (2016) no.12, 691 [[arXiv:1607.04538](#) [[hep-ph](#)]].
- [45] A. Denner and M. Pellen, *NLO electroweak corrections to off-shell top-antitop production with leptonic decays at the LHC*, JHEP **1608** (2016) 155 [[arXiv:1607.05571](#) [[hep-ph](#)]].
- [46] P. F. Duan, Y. Zhang, Y. Wang, M. Song and G. Li, *Electroweak corrections to top quark pair production in association with a hard photon at hadron colliders*, Phys. Lett. B **766** (2017) 102 [[arXiv:1612.00248](#) [[hep-ph](#)]].
- [47] Z. Bern, L. J. Dixon, F. Febres Cordero, S. Höche, H. Ita, D. A. Kosower and D. Maitre, *Ntuples for NLO Events at Hadron Colliders*, Comput. Phys. Commun. **185** (2014) 1443 [[arXiv:1310.7439](#) [[hep-ph](#)]].
- [48] J. Alwall *et al.*, *A Standard format for Les Houches event files*, Comput. Phys. Commun. **176** (2007) 300 [[hep-ph/0609017](#)].
- [49] I. Antcheva *et al.*, *ROOT: A C++ framework for petabyte data storage, statistical analysis and visualisation*, Comput. Phys. Commun. **180** (2009) 2499 [[arXiv:1508.07749](#) [[physics.data-an](#)]].